



**UNIVERSIDAD DE INVESTIGACIÓN DE TECNOLOGÍA
EXPERIMENTAL YACHAY**

Escuela de Ciencias Químicas e Ingeniería

**TÍTULO: Removal of Crystal Violet Dye from Aqueous Solution
Using Ecuadorian Black Sands as Photocatalytic Adsorbents**

Trabajo de integración curricular presentado como requisito para la
obtención del título de Química

Autor:

Gómez Gómez Johanna Mishell

Tutor:

Ph.D Palma Cando Alex Uriel

Urcuquí, febrero 2020

SECRETARÍA GENERAL
(Vicerrectorado Académico/Cancillería)
ESCUELA DE CIENCIAS QUÍMICAS E INGENIERÍA
CARRERA DE QUÍMICA
ACTA DE DEFENSA No. UITEY-CHE-2020-00002-AD

En la ciudad de San Miguel de Urcuquí, Provincia de Imbabura, a los 21 días del mes de febrero de 2020, a las 11:00 horas, en el Aula CHA-01 de la Universidad de Investigación de Tecnología Experimental Yachay y ante el Tribunal Calificador, integrado por los docentes:

Presidente Tribunal de Defensa	Dr. CAETANO SOUSA MANUEL , Ph.D.
Miembro No Tutor	Mgs. DE LIMA ELJURI, LOLA MARIA
Tutor	Dr. PALMA CANDO, ALEX URIEL , Ph.D.

Se presenta el(la) señor(ita) estudiante GOMEZ GOMEZ, JOHANNA MISHELL, con cédula de identidad No. 1724622798, de la ESCUELA DE CIENCIAS QUÍMICAS E INGENIERÍA, de la Carrera de QUÍMICA, aprobada por el Consejo de Educación Superior (CES), mediante Resolución RPC-SO-39-No.456-2014, con el objeto de rendir la sustentación de su trabajo de titulación denominado: Removal of crystal violet dye from aqueous solution using ecuadorian black sands as photocatalytic adsorbents, previa a la obtención del título de QUÍMICO/A.

El citado trabajo de titulación, fue debidamente aprobado por el(los) docente(s):

Tutor	Dr. PALMA CANDO, ALEX URIEL , Ph.D.
Co - Tutor	Dr. VILORIA VERA, DARIO ALFREDO , Ph.D.

Y recibió las observaciones de los otros miembros del Tribunal Calificador, las mismas que han sido incorporadas por el(la) estudiante.

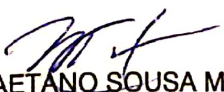
Previamente cumplidos los requisitos legales y reglamentarios, el trabajo de titulación fue sustentado por el(la) estudiante y examinado por los miembros del Tribunal Calificador. Escuchada la sustentación del trabajo de titulación, que integró la exposición de el(la) estudiante sobre el contenido de la misma y las preguntas formuladas por los miembros del Tribunal, se califica la sustentación del trabajo de titulación con las siguientes calificaciones:

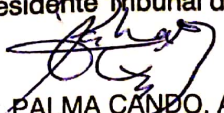
Tipo	Docente	Calificación
Tutor	Dr. PALMA CANDO, ALEX URIEL , Ph.D.	9,8
Miembro Tribunal De Defensa	Mgs. DE LIMA ELJURI, LOLA MARIA	9,8
Presidente Tribunal De Defensa	Dr. CAETANO SOUSA MANUEL , Ph.D.	9,6

Lo que da un promedio de: 9.7 (Nueve punto Siete), sobre 10 (diez), equivalente a: APROBADO

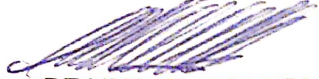
Para constancia de lo actuado, firman los miembros del Tribunal Calificador, el/la estudiante y el/la secretario ad-hoc.



GOMEZ GOMEZ, JOHANNA MISHELL
Estudiante


Dr. CAETANO SOUSA MANUEL , Ph.D.
Presidente Tribunal de Defensa


Dr. PALMA CANDO, ALEX URIEL , Ph.D.
Tutor




Mgs. DE LIMA ELJURI, LOLA MARIA
Miembro No Tutor


ESCOBAR LANDAZURI, ANA MARIA
Secretario Ad-hoc



AUTORÍA

Yo, **JOHANNA MISHELL GÓMEZ GÓMEZ**, con cédula de identidad 1724622798, declaro que las ideas, juicios, valoraciones, interpretaciones, consultas bibliográficas, definiciones y conceptualizaciones expuestas en el presente trabajo; así cómo, los procedimientos y herramientas utilizadas en la investigación, son de absoluta responsabilidad de el/la autora (a) del trabajo de integración curricular. Así mismo, me acojo a los reglamentos internos de la Universidad de Investigación de Tecnología Experimental Yachay.

Urcuquí, febrero y 2020.



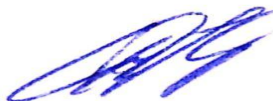
Johanna Mishell Gómez
CI: 1724622798

AUTORIZACIÓN DE PUBLICACIÓN

Yo, **JOHANNA MISHELL GÓMEZ GÓMEZ**, con cédula de identidad 1724622798, cedo a la Universidad de Tecnología Experimental Yachay, los derechos de publicación de la presente obra, sin que deba haber un reconocimiento económico por este concepto. Declaro además que el texto del presente trabajo de titulación no podrá ser cedido a ninguna empresa editorial para su publicación u otros fines, sin contar previamente con la autorización escrita de la Universidad.

Asimismo, autorizo a la Universidad que realice la digitalización y publicación de este trabajo de integración curricular en el repositorio virtual, de conformidad a lo dispuesto en el Art. 144 de la Ley Orgánica de Educación Superior

Urququí, febrero y 2020.



Johanna Mishell Gómez Gómez
CI: 1724622798

Dedicatoria

To all my family that gives me the support during all this time but in special for my mom Blanca Gómez and my dad Gustavo Gómez because without them I would not be the person that I am.

To my mom, Blanca, thank you to gives me life, for all the effort that makes every day in order to impulse me to reach my dreams.

To my dad, Gustavo, thank you for teaches me that the work is the unique way to obtain anything and give me everything that I needed.

To all my friends that accompanied me in my university life.

Johanna Mishell Gómez Gómez

Agradecimiento

I would like to express my gratitude to one and all that helped me and motivated me during my project. First of all, I would like to thank Applied Research Group in Materials and Processes (GIAMP).

I would like to thank Dr. Martha Romero and her team from the INPC Laboratory for the results of Energy-Dispersive x-ray Spectroscopy (EDS) and X-Ray Diffraction (XRD).

Next, I would like to thank Ph.D. Alex Palma, Ph.D. Manuel Caetano y MSc. Lola de Lima for guiding me through this work and providing me with valuable information and knowledge during each stage of the project. They always helped me with all the problems during this work. Their encouragement and efforts led this project to successful completion.

I would like to thank Ph.D. Jorge Toro for his contribution to information about samples of sands used in this work.

I am thankful to my friend Dayanna Vera for her assistance, help, and support in my work, which gave me information about the sand that I used in this work.

Johanna Mishell Gómez Gómez

Resumen

En el presente trabajo, se llevó a cabo la remoción (decoloración) del colorante violeta cristal (VC) en solución acuosa, mediante el proceso adsorción y fotocatalisis integrados, utilizando dos arenas negras de diferentes partes del Ecuador, de Mompiche y del volcán Quilotoa. Las muestras de arena que se usaron como adsorbentes fotocatalíticos se caracterizaron por sus propiedades ópticas (Band-Gap) utilizando espectroscopía de reflectancia difusa UV-Vis. Los valores determinados están en el rango apropiado para un fotocatalizador en comparación con los reportados por la literatura. Los experimentos proporcionaron valores de band-gap de 3.37 eV y 3.68 eV para Mompiche y Quilotoa respectivamente. La concentración de peróxido de hidrógeno, pH e irradiación de luz fueron optimizados por un diseño experimental de 2^n para la eliminación de VC con SEM-205 y SXQ-102. Se determinó que el valor de pH óptimo para la adsorción de colorante era 8. Los espectros de absorción UV-Vis a diferentes intervalos de tiempo mostraron que en el proceso de adsorción con SEM-205 y SXQ-102 solo hay una disminución en los picos que confirma su naturaleza absorbente. Los espectros UV-Vis del proceso integrado de fotocatalisis y adsorción con SEM-205 y SXQ-102 mostraron la aparición de nuevos picos en el espectro, lo que significaba la aparición de intermediarios y subproductos. Se observó que, en condiciones optimizadas, el 97,1% de tinte se podía eliminar de la solución en 2 horas utilizando arena de Mompiche (SEM-205).

Palabras Clave:

Arena negra, Adsorción y Fotocatálisis Integrada (IPCA), Cristal violeta, Isotermas de adsorción, Modelos Cinéticos.

Abstract

In the present work, the removal (discoloration) of the crystal violet dye (CV) in aqueous solution was carried out, through the Integrated Photocatalysis and Adsorption (IPCA) process, using two black sands from different parts of Ecuador, Mompiche and the Quilotoa volcano. Sand samples used as photocatalytic adsorbents are characterized by their optical properties (Band-Gap) using UV-Vis diffuse reflectance spectroscopy. The determined values are in the appropriate range for a photocatalyst in comparison with those reported by the literature. The experiments provided band-gap values of 3.37 eV and 3.68 eV for Mompiche and Quilotoa respectively. Concentration of hydrogen peroxide, pH and light irradiation were optimized by an 2^n experimental design for the removal of CV on SEM-205 and SXQ-102. Optimum pH value for dye adsorption was determined to be 8. The UV-Vis absorption spectra at different time intervals showed that in the adsorption process with SEM-205 and SXQ-102 there is only a decrease in peaks which confirms its absorbent nature. The UV-Vis spectra of the integrated photocatalysis and adsorption process with SEM-205 and SXQ-102 showed the appearance of new peaks in the spectrum which meant the appearance of intermediaries and by-products. It was seen that under optimized conditions, 97.1% dye could be removed from the solution in 2 hours using Mompiche's sand (SEM-205).

Key Words:

Black sand, Integrated Photocatalysis and Adsorption (IPCA), Crystal violet, Dye removal, Adsorption Isotherms, Kinetics models

Contents

1	Introduction	1
1.1	Problem Statement	3
2	Objectives	4
2.1	General Objective	4
2.2	Specific Objectives	4
3	Experimental section	5
3.1	Materials and Reagents	5
3.2	Instruments	5
3.3	Methodology	6
3.3.1	Type of Investigation and Sampling Process	6
3.3.1.1	Type of Investigation	6
3.3.2	Sands	6
3.3.3	Crystal Violet Dye	9
3.3.4	Sands characterization	10
3.3.4.1	UV-Vis diffuse reflectance spectroscopy (UV-Vis DRS)	10
3.3.5	Dye characterization	11
3.3.5.1	UV-Vis Spectroscopy	11
3.3.5.2	Fourier Transform Infrared Spectrophotometry (FTIR)	11
3.3.6	Experimental Design	11
3.3.6.1	Factors selection	11
3.3.6.2	Selection of the experimental design and its matrices	12
3.3.7	Processes used to study the removal of the crystal violet dye using Ecuadorian Sands.	13
3.3.8	Kinetics studies	16
3.3.9	Adsorption isotherms	16
4	Results and Discussion	18

4.1	Characterization of Sands	18
4.1.1	UV-Vis diffuse reflectance spectroscopy (UV- Vis DRS)	18
4.2	Crystal Violet Dye Characterization	19
4.2.1	UV-Vis Spectroscopy	19
4.2.2	Fourier Transform Infrared Spectrophotometry (FTIR)	20
4.3	Experimental Design	21
4.4	Kinetics of IPCA and Adsorption with SXQ-102 and SEM-205	28
4.4.1	Kinetics with SXQ-102 of best results of IPCA and adsorption processes.	28
4.4.2	Kinetics with SEM-205 of best results of IPCA and adsorption processes.	29
4.5	UVVis absorption spectra	31
4.6	Adsorption Isotherms	33
4.7	Kinetic Study	37
5	Conclusions	43
6	Recommendations	44
	Appendices	56
A	Appendix 1.	56
A.1	Crystal Violet Dye	56
A.2	Techniques of wastewater treatment	57
A.3	Adsorption	58
A.4	Advanced Oxidation Processes (AOPs)	58
A.4.1	Photo-Fenton and Heterogeneous Photo-Fenton	59
A.4.2	Heterogeneous Photocatalysis with TiO_2	60
A.5	Integrated Photocatalyst Adsorbents (IPCA)	61
A.6	Black Sands	62
A.6.1	Deposits of Black sands in Ecuador	62
B	Appendix 2.	63
C	Appendix 3.	66

D Appendix 4.	69
E Appendix 5.	71
F Appendix 6.	75
G Appendix 7	76
G.1 Adsorption isotherms	76
G.1.0.1 Langmuir Model	76
G.1.0.2 Freundlich Model	77
G.1.0.3 Temkin Model	78
G.1.0.4 Dubinin-Radushkevich (D-R) model	78
G.2 Kinetic Study	79
G.2.0.1 Pseudo First-Order Kinetic Model	80
G.2.0.2 Pseudo Second Order Kinetic Model	80
G.2.0.3 Elovich Kinetic Model	81
G.2.0.4 The Intraparticle Diffusion Model (Weber-Morris)	81
H Appendix 8.	83

List of Figures

1	EDS analysis of SXQ-102(a) and SEM-205(b)	8
2	A processes flow diagram to study the removal of the crystal violet dye using Ecuadorian Sands.	15
3	UV-Vis absorption spectrum for magnetically enriched and grounded black sand fractions of SXQ-102(a) and SEM-205(b).	18
4	Tauc plot using the UV-Vis DRS of SXQ-102(a) and SEM-205(b).	18
5	UV-Vis spectrum of CV dye	19
6	FTIR spectrum of CV dye.	20
7	Q-Q plot of experimental design.	23
8	Q-Q plot of experimental design (SXQ-102).	25
9	Q-Q plot of experimental design (SEM-205).	27
10	Kinetics for SXQ-102 IPCA and Adsorption.	28
11	CV dye in solution and Discoloration by SXQ-102 after 2 hours.	29
12	Kinetics for SEM-205 IPCA and Adsorption.	30
13	CV dye in solution and Discoloration by SXQ-102 after 2 hours.	30
14	Absorption spectra of the initial CV solution and after 10, 20, 30, 40, 50, 60, 70, 80, 100, 120 min. Conditions: $[CV]_0=40$ ppm, pH=8, Sand= SXQ-102(a) and SEM-205(b). (Adsorption)	31
15	Absorption spectra of the initial CV solution and after 10, 20, 30, 40, 50, 60, 70, 80, 100, 120 min. Conditions: $[CV]_0=40$ ppm, pH=8, $[H_2O_2]$, Irradiation, Sand= SXQ-102(a) and SEM-205(b). (Integrated Photocatalysis and Adsorption (IPCA))	32
16	Relation between amounts of CV adsorbed at equilibrium (q_e) using different concentrations of SXQ-102 and SEM-205	33
17	Linear Langmuir (a) and Freundlich (b) model for adsorption of Crystal Violet over SEM-205 and SXQ-102.	35
18	Linear Temkin (a) and Dubinin-Radushkevich (b) model for adsorption of Crystal Violet over SEM-205 and SXQ-102.	36

19	Pseudo-First-order (a) and Pseudo-second-order model (b) for removal of crystal violet dye by SEM-205 and SXQ-102.	40
20	Elovich (a) and Weber-Morris model (b) for removal of crystal violet dye by SEM-205 and SXQ-102.	41
21	Structure of Crystal Violet	56
22	Semiconductors photocatalytic mechanism.. . . .	61
23	Schematic integrated adsorption and degradation of CV over Sands under UV-visible-light illumination.	62
24	Relation between amounts of CV adsorbed at equilibrium (q_e) using different concentrations of SXQ-102 and SEM-205	83

List of Tables

1	Materials and reagents necessary for the research	5
2	Information about SXQ-102 sand [32].	6
3	Information about SEM-205 sand [32].	7
4	Results of X-ray diffraction of SXQ-102	7
5	Results of X-ray diffraction of SEM-205	8
6	Weight percentage of oxides in SEM-205 and SXQ-102 sands.	9
7	Characteristics of Crystal Violet	10
8	Levels of the variables involved in the experiment	12
9	Matrix of coded variables factorial design 2^4	12
10	Band-gap values of the sands.	19
11	Percentage of discoloration and degradation of CV in the Runs Performed in the Experimental Design.	21
12	Analysis of the variance for the removal of crystal violet dye.	22
13	Results of discoloration percentages with SEM-205 according to the design of factorial experiments.	24
14	Analysis of the variance for the response percentage of discoloration using SEM- 205 sand	24
15	Results of discoloration percentages with SXQ-102 according to the design of factorial experiments.	26
16	Analysis of the variance for the response percentage of discoloration using SXQ- 102 sand	26
17	Best results of IPCA and adsorption processes with SXQ-102 obtained from experimental design	28
18	Best results of IPCA and adsorption processes with SEM-205 obtained from experimental design	29
19	Isotherm models obtained from linear solvation	34
20	Comparison of kinetic models	39
21	Composition of commercial Crystal Violet	56

22	Classification of AOPs	59
23	Table of Classification of Dyes in Textile Industry	63
24	Photochemical and Non-photochemical processes	66
25	Techniques of wastewater treatment	69
26	Previuos study on IPCA for organic contaminants degradation in waste water treatment	71

1 Introduction

Around 2000 million people live in countries that suffer severe water scarcity [1]. In Ecuador, INEC studies show that 70% of Ecuadorians have access to improved water sources, while the remaining 30% use natural watersheds that are generally contaminated with waste from agricultural and industrial activity, seriously affecting for them that consume it [2]. For this reason, it is extremely urgent to seek effective and economical solutions for the treatment of these natural sources.

The textile industry is one of the most polluting of the environment, generating 20% of wastewater worldwide [3]. Ecuador textile sector is one of the largest employment generators [4] being the provinces with the highest number of establishments Pichincha, Guayas, Tungurahua, Azuay, and Imbabura [5], 80% of these establishments do not invest in environmental protection, generating waste that goes directly to the public sewer network and then to rivers without no type of treatment [6].

These discharges have a large amount of non-biodegradable organic compounds, especially textile dyes that are highly soluble in water, making them difficult to remove by conventional methods like flocculation, adsorption or biological processes. [7].

One of the most used textile dyes is crystal violet dye also called gentian violet or methyl violet 10B. It is also widely used in cosmetics, veterinary and is an antifungal and antibacterial agent [8]. On the other hand, it has been reported that crystal violet dye is a recalcitrant molecule that persists in the environment for long periods, affecting aquatic and terrestrial life [9]. Studies reveal that they have carcinogenic effects. Due to these adverse effects and because it continues to be widely used in the industry, it was chosen as a the target molecule in this work [10], (Appendix A.1 and B).

There have been many methods used for the degradation of dyes and the most important for this work are adsorption and photocatalysis Appendix A.2 and C.

Adsorption is a physical technique, which is a promising treatment option for pollutant removal due to its efficiency, simplicity, and it is inexpensive and not toxic [11, 12]. In the process of adsorption, the dye's molecules get separated from the liquid phase and gets accumulated on the adsorbent [13]. This occurs due to an attractive force between the adsorbent and the

dye's molecules. When solely utilized, this method is unable to eliminate or destroy the pollutants completely. Various adsorbents have been reported in published works for the removal of pollutants such as activated carbon, clays, zeolite, and polymeric adsorbents [14, 15, 16, 17].

Furthermore, the photocatalytic process is an advanced oxidation process characterized by the formation of OH^\bullet radicals in the presence of a photocatalyst, a source of irradiation and hydrogen peroxide. These hydroxyl radicals are responsible for the degradation of organic compounds to carbon dioxide and water[20]. The most studied photocatalysts by the scientific community are: Titanium Oxide (TiO_2) and Iron salts [Fe(II) and Fe(III)]

The photocatalytic activity depends on the capacity of the photocatalyst to promote an electron from the valence band to the conduction band creating a hole that generates hydroxyl radicals, the additional electron in the conduction band can also interact with the dissolved oxygen to create radicals. As the energy of the photocatalyst band-gap decreases, its optical response shifts to higher excitation lengths. So if the band-gap is narrow, photocatalyst can be used as a source of visible light irradiation. The combination of these 2 methods results in a novel method called Integrated Photocatalysis and Adsorption (IPCA)[20] and Appendix A.4.

The integrated photocatalysis and adsorption technique brings many benefits to the treatment of wastewater, it not only preserves the important characteristics of each of them but also overcomes the disadvantages of each technique [21]. Surprisingly, the number of publications referring to this process is very limited, approximately only 13.7 % of the total publications in photocatalysis for the treatment of wastewater made from 1989 to 2018. This reflects that more efforts are needed to establish this technique for wastewater treatment applications [22], (Appendix A.5 and D).

Studies of dyes degradation use zeolite as an adsorbent, most of the photocatalysts are made up of iron and titanium oxides for their narrow band-gap, so for having an ideal photocatalytic adsorbent should have iron and titanium oxides such as ilmenite or hematite and aluminum and silicon oxides such as zeolite.

In this work, we use black sands as photocatalytic adsorbents in the degradation of crystal violet dye. Black sands are natural combinations of minerals like aluminosilicates minerals composed of iron and titanium oxides [24]. Studies in the photocatalytic activity of black sands of Colombia magnetically enriched show a percentage of 99% discoloration in 50 min

[25]. Other studies concerning the adsorbent activity of sands of the United States show percentages of discoloration between 60 and 70% [26]. Taking into account previous studies and its composition one might think that it is possible to use black sands as photocatalytic adsorbents [27, 28].

Studies in black sands of Ecuador show the existence of minerals composed of iron and titanium oxides, so it can be assumed that they are ideal for the integrated adsorption and photocatalysis process [29, 30, 31] and Appendix A.6.

1.1 Problem Statement

Dyes are widely used in various industries such as textile, cosmetics, paper, etc. The wastewater generated by these industries are discharged into the freshwater systems without sufficient treatment, creating severe pollution problems. Most dyes are toxic, mutagenic and/or carcinogenic thus affecting the aquatic organisms and human health. Hence, the removal of these dyes from effluents is essential. Various methods have been reported for the elimination of dyes from wastewater, but the major of them are not effective and are expensive.

This research is focused on the necessity to develop and low-cost and effective alternative treatment. The present investigation was conducted with the prime objective to evaluate the feasibility of using two Ecuadorian black sands as photocatalytic adsorbents for the effective treatment of one cationic dye (crystal violet) from aqueous solution.

2 Objectives

2.1 General Objective

To perform the removal of the crystal violet dye in aqueous solution through the integrated photocatalysis and adsorption process using two black sands from different parts of Ecuador.

2.2 Specific Objectives

- To evaluate the potential of the natural mineral that will be used in dye removal study based on its physicochemical and optical characteristics.
- To determine the Band-Gap value of both sand samples to confirm their photocatalytic nature.
- To determine the influence of four reaction variables: concentration of hydrogen peroxide, pH, catalyst and irradiation, on the removal of dye using a factorial experiment design.
- To examine the applicability of the various isotherm models to understand the nature of dye-adsorbent interaction
- To study the kinetics of the adsorbent process by fitting the kinetic data in various kinetic models.

3 Experimental section

3.1 Materials and Reagents

Table 1: Materials and reagents necessary for the research

Material	Reagents
Beakers	Crystal Violet dye
Spatula	Hydrogen peroxide
Magnetic stirrer	Citrate Buffer (pH 3.0 and 8)
Aluminum foil	Distilled water
Graduated cylinder	
Pipette	
Volumetric flask	
Pipette tips	
Test tube	
Test-tube rask	

3.2 Instruments

- pH meter
- Analytical Balance
- UV Chamber at 365 nm
- Hot plate stirrer
- UV-Vis Spectrophotometer
- Lambda 1050 UV/Vis/NIR spectrometer of the Perkin Elmer brand
- Praying mantis accesory
- The Agilent Cary 630 FTIR Spectrometer

3.3 Methodology

3.3.1 Type of Investigation and Sampling Process

Experimental wastewater treatment processes for the removal of dyes by integrated photocatalysis and adsorption processes using black sands from Ecuador as photocatalytic adsorbents was carried out with the crystal violet dye as the target molecule.

3.3.1.1 Type of Investigation

An experimental investigation was carried out, to determine the optimal conditions for the degradation of the violet crystal dye dissolved in water, in a 100 ml capacity reactor within a UV radiation chamber, the degradation was mediated by two different sand catalysts, oxidizing agent hydrogen peroxide and UV light.

3.3.2 Sands

The black sand samples used in this work were from two different parts of Ecuador, one of them was obtained from an intermittent river environment, reworked from pyroclastic flows, rich in iron, taken from the southeast of the Quilotoa - Cotopaxi Volcano. the second sand was originated from an iron ore deposit in the upper part of Mompiche - Esmeraldas beach. These samples were provided by the INÉDITA project of Ferruginous and Titaniferous Sands of Ecuador as adsorbents of acid gases in the hydrocarbon industry.

Table 2: Information about SXQ-102 sand [32].

2	Identification	SXQ-102	
	code	180716.2	
Volcanoclastic sands, in intermittent river environment, reworked from pyroclastic flows collected in the southeastern of the Quilotoa Volcano in the province of Cotopaxi			

Table 3: Information about SEM-205 sand [32].

11	Identification	SEM-205
	code	180731.2a
Quartz sand from the high tide area at the top of Mompiche beach in the province of Esmeraldas		

The sands were previously characterized by the Research Group Applied in Materials and Processes (GIAMP), Characterization techniques used were: X-Ray Diffraction (XRD) using an X-Ray Diffractometer BRUKER D8-ADVANCE with Cu anode $\lambda=1.5406 \text{ \AA}$ and Energy-Dispersive X-ray Spectroscopy (EDS) and gave the following results.

A summary of the X-ray diffraction data deduced from the powder pattern of SXQ-102 and SEM-205 sands is shown in tables 4 and 5

Ilmenite, Anatase (titanium dioxide) and Silicon Oxide are present in Quilotoa Sand. The two former are reported as photocatalyst and the latter as an adsorbent (Appendix E). With this information, it could be concluded that this sand can be used as photocatalytic adsorbents. But in addition to these minerals previously reported, it can be seen that there are others that have silicon and aluminum in its chemical composition that have also been reported as adsorbents (Table 4).

Table 4: Results of X-ray diffraction of SXQ-102

SXQ-102	
Name	Formula
Hematite	Fe_2O_3
Ilmenite	FeTiO_3
Silicon oxide (Quartz low)	SiO_2
Albite	$\text{NaAlSi}_3\text{O}_8$
Anatase	TiO_2

As shown in table 5, the sands of Mompiche beach there is Hematite which has adsorbent and photocatalytic nature. There is also a considerable amount of silicon oxides characteristic for its adsorbent nature.

Table 5: Results of X-ray diffraction of SEM-205

SEM-205	
Name	Formula
Quartz	SiO ₂
Ilmenite	FeTiO ₃
Aegirine	NaAlSi ₃ O ₆

The analysis with EDS yielded information about the oxides that make up each sand. Only the amount of oxides present is known because the samples were mixed with cellulose so that its elemental composition was not obtained. The percentages of iron, titanium, silicon and aluminium oxides, present in both sands, are shown in table 6. These oxides are important as integrated photocatalyst and adsorbents.

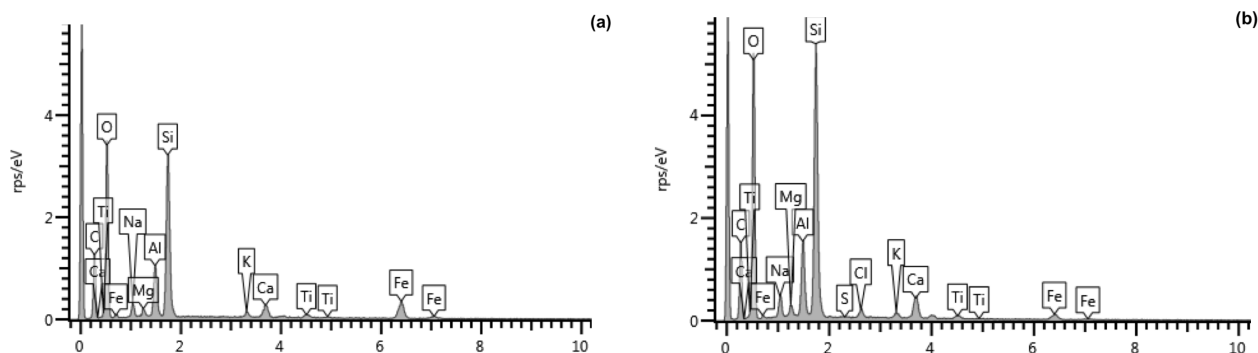


Figure 1: EDS analysis of SXQ-102(a) and SEM-205(b)

Table 6: Weight percentage of oxides in SEM-205 and SXQ-102 sands.

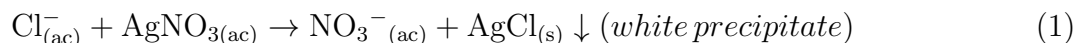
Oxides	Sands	
	SXQ-102	SEM-205
Al	14.33 %	13.74 %
Si	51.35 %	57.05 %
Ti	1.61 %	1.63 %
Fe	16.8 %	6.73 %
Others	15.91 %	21.59 %

The silicon oxides in SXQ-102 and SEM-205 are the main oxides with 51.35% and 57.05% mean content respectively. Aluminum oxides are found with concentration of 14.33% and 13.74% respectively.

On the other hand, the percentage of iron oxides in the SXQ-102 sand are much higher (16.8%) compared to the SEM-205 sand (6.73%). The percentage of titanium oxides are similar for both samples, with 1.61% for SXQ-102 and 1.63% for SEM-205.

The sands were dried in the open air. Water loss was followed as a function of time. Then, they are washed with distilled water until pH of 7 was achieved, and all the mater-soluble impurities, such as chlorides that can interfere with the remove process were removed.

A silver nitrate solution was used to determine chloride ions by precipitation eq (1)[33, 34].



Finally, the samples were dried at 80°C for 24 hours.

3.3.3 Crystal Violet Dye

Chloride salt of crystal violet (CV; Cl 42555; Basic Violet 3; hexamethylpararosaniline chloride; Methyl Violet 10B) was obtained from a local distributor Liderquim. The material specifications provided by the manufacturer are found in the Table 7.

Table 7: Characteristics of Crystal Violet

Product name	Gentian violet or Crystal violet
Molecular formula	$C_{25}H_{30}ClN_3$
Molecular weight	407.99 g/mol
Melting point	205 °C
Boiling point	560.86 °C
Density	1.19 g/cm^3 (20°C)
Strength	200%
Color shade	Comply with the standard
Moisture	3% Max
Insolubility	1% Max

3.3.4 Sands characterization

3.3.4.1 UV-Vis diffuse reflectance spectroscopy (UV-Vis DRS)

Using UV-Vis spectroscopy it is possible to quantify the electronic transitions that the molecules undergo when they are irradiated with electromagnetic radiation from the Visible (Vis), near-Ultraviolet (UV) and Near-Infrared (NIR) region of the electromagnetic spectrum (wavelength between 380nm and 780nm). The sand samples were magnetically enriched and ground with the help of an agate mortar. They were mixed with barium sulfate $BaSO_4$ standard at different proportions. DRS spectra from standard and the mixed samples were obtained. To perform the UV-Vis analysis, a Lambda 1050 Spectrometer with Praying mantis accessory was used. Each sample were mixed with $BaSO_4$ and placed in a small metal cell aligned to the incident beam of the equipment, the wavelength range studied was 200 to 3500 nm.

The Kubelka-Munk function $F(R)$ (Appendix F) was obtained from the absorbance data. Graphing the group of values of $[F(R)h\nu]^n$ vs $h\nu$ (Tauc plot) and extrapolating a straight line that crosses the axis of the coordinates gave the value of band-gap.

3.3.5 Dye characterization

3.3.5.1 UV-Vis Spectroscopy

The Crystal Violet (CV) dye sample was characterized by UV-Vis spectroscopy using 1 cm wide quartz cells. A Lambda 1050 UV/VIS/NIR spectrometer of the Perkin Elmer brand was used, the wavelength range from 190 nm to 800 nm. Crystal violet showed maximum absorbance at 543.9 nm. This value was used for the study of dye removal. In addition to the spectrum obtained, the structure of the dye was analyzed.

3.3.5.2 Fourier Transform Infrared Spectrophotometry (FTIR)

The FTIR spectrum was obtained using The Agilent Cary 630 FTIR spectrometer and Micro-Lab software, measured in the wavelength range from 4000 to 350 nm. 0.5 grams of the solid crystal violet dye was used and placed in the plate of the FTIR. With this analysis, it was possible to obtain information on the chemical structure of the crystal violet dye.

3.3.6 Experimental Design

3.3.6.1 Factors selection

In order to identify the significant main factors(variables) that may impact the adsorption and photocatalysis processes, a full 2^n factorial design was chosen, where n is the number of factors considered and two the number of levels.

This design allows obtaining information on the four factors or variables in each experiment, being more efficient and containing more information (interaction between factors) than a design where we change one factor at a time while the rest remains constant. The variables selected for the discoloration process are:

- Irradiation
- Catalyst
- pH
- Hydrogen peroxide

3.3.6.2 Selection of the experimental design and its matrices

Each variable in this design has two levels and its experiments propose all possible combinations that can be given at each level of one variable with other levels of the other variables. In table 8 we can see the operational and coded (+1,-1) levels of each of the factors. These values were chosen using data reported and previously experiments. The catalyst concentration (sand) was 0.33 g/ml. Therefore, 16 experiments were performed, in addition 6 replicates of 2 experiments were carried out to be able to verify the reproducibility of the dye removal processes and estimate the error of the model parameters. The 22 experiments are displayed in table 9 in conventional order, The experiments were performed randomly.

Table 8: Levels of the variables involved in the experiment

Variables	Level (-1)	Level (+1)
Catalyst (Sand)	SEM-205	SXQ-102
pH	3	8
Hydrogen Peroxide (H ₂ O ₂)	0	1 M
Irradiation	NO	365 nm

In Table 9 we can see the 22 experiments with the different combinations possible of levels, the second column begin with a negative level after with a positive level and them continue to alternate. The matrix of randomized categorical variables was obtained through the Excel program which was coded according to Table 9.

Table 9: Matrix of coded variables factorial design 2⁴

Treatments	Sand	pH	H ₂ O ₂	Irradiation
1	-1	-1	-1	-1
2	+1	-1	-1	-1
3	-1	+1	-1	-1
4	+1	+1	-1	-1
5	-1	-1	+1	-1
6	+1	-1	+1	-1

7	-1	+1	+1	-1
8	+1	+1	+1	-1
9	-1	-1	-1	+1
10	+1	-1	-1	+1
11	-1	+1	-1	+1
12	+1	+1	-1	+1
13	-1	-1	+1	+1
14	+1	-1	+1	+1
15	-1	+1	+1	+1
16	+1	+1	+1	+1
17	-1	+1	+1	-1
18	-1	+1	+1	-1
19	-1	+1	+1	-1
20	+1	+1	+1	-1
21	+1	+1	+1	-1
22	+1	+1	+1	-1

3.3.7 Processes used to study the removal of the crystal violet dye using Ecuadorian Sands.

The procedure that was used to carry out the different laboratory scale experiments is described below: The pH values of the CV dye sample were adjusted with citrate buffers of different pH. To adjust the pH to 3, 1 ml of citrate buffer was used and pH 8 0.5, ml of citrate buffer was used.

For the preparation of the citrate buffer at pH 3 and 8, 500 ml of a citric acid solution 0.1 M was prepared with 10.5069 g and a sodium citrate solution 0.1 M was prepared with 12.9035 g. For the buffer at pH 3, 150 ml of the citric acid solution and 106.18 ml of sodium citrate solution were mixed and adjusted with sulfuric acid solution 0.1 M and sodium hydroxide 0.1 M. For the buffer at pH 8, 6 ml of the citric acid solution and 238.86 ml of sodium citrate solution

were mixed, similarly, it was adjusted using solutions of sulfuric acid and sodium hydroxide.

1. 12.5 ml of the CV dye was placed in a 100 ml beaker.
2. The pH was measured and adjusted to the necessary pH.
3. 5g of sand and 2.5 ml of hydrogen peroxide was placed at the same time.
4. The beaker was placed for 2 hours in a reaction chamber equipped with a UV lamp 365 nm. In the case that the experiment was without irradiation, it was necessary to wrap it with aluminum foil to prevent the light from entering the chamber.
5. After 2 hours, 3 ml of sample was taken in a quartz cell to measure the absorbance in a UV-Vis Spectrophotometer at wavelength 543.9 nm.
6. With the absorbance measurements obtained, the percentage of discoloration was calculated using the following equation:

$$\%Discoloration = \frac{A_0 - A_{2h}}{A_0} \cdot 100 \quad (2)$$

Where A_0 is the absorbance at initial time, and A_{2h} is the absorbance after 2 hours.

In figure 3 a processes flow diagram is displaying.

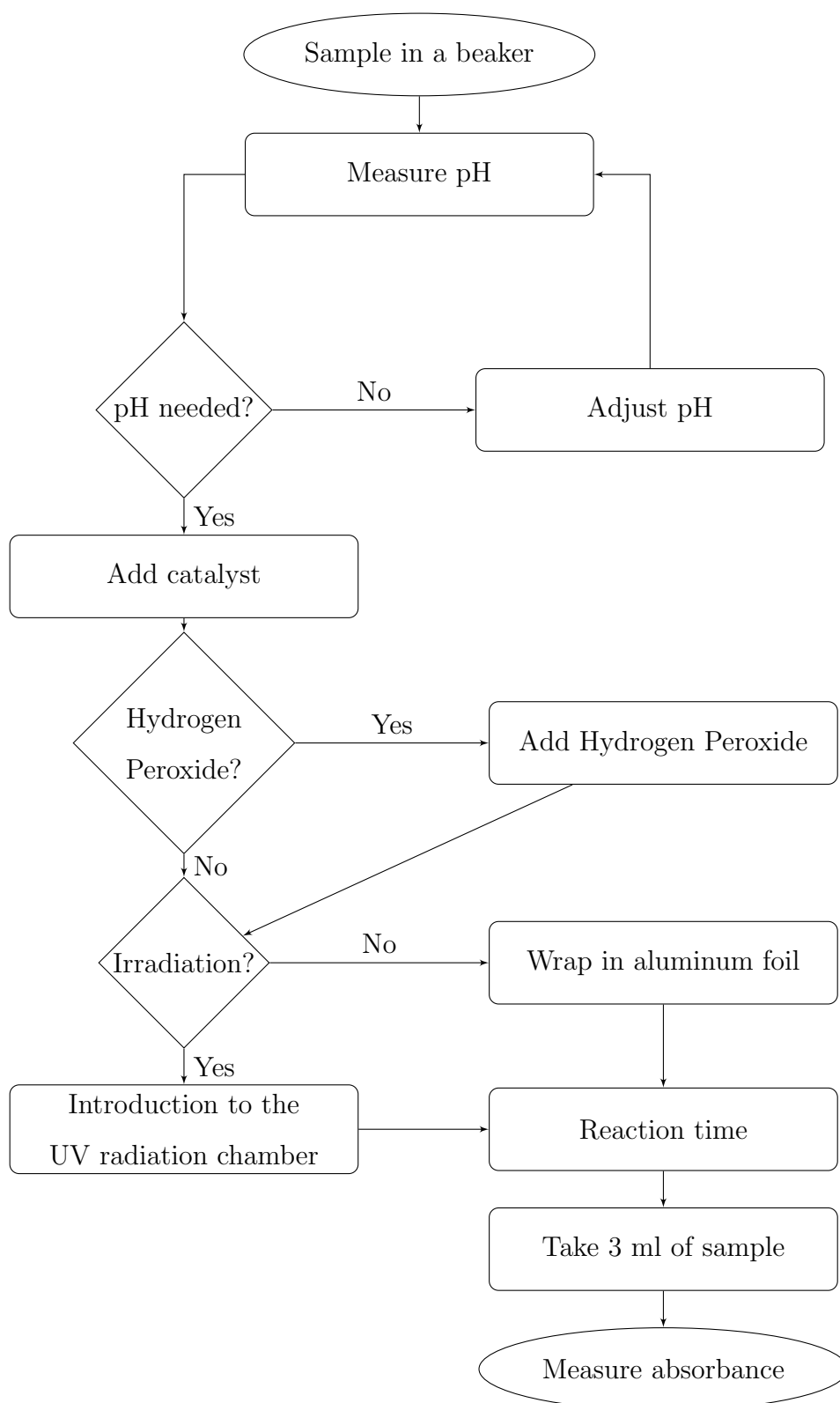


Figure 2: A processes flow diagram to study the removal of the crystal violet dye using Ecuadorian Sands.

3.3.8 Kinetics studies

Kinetics studies were performed on 100 ml beakers with the best parameters obtained for the adsorption process (without the presence of irradiation nor hydrogen peroxide) in the experimental design previously performed. The concentration of the CV dye was 40 mg/L. The process flow for this study was the same as that used in the experimental design. During 2 hours, 3 ml samples were collected in quartz cuvettes to measure their absorbance in the Spectrophotometer at required time intervals, at 0, 12, 24, 36, 48, 60, 72, 95, 120 min, with the absorbance values obtained, the percentages of discoloration were calculated using the equation (2).

Kinetic models were used to determine the rate of the adsorption process. The kinetic data for the various adsorbate-adsorbent systems studied in the present work were analysed with four different kinetic models, namely, pseudo-first order, pseudo-second order, intraparticle diffusion (Wever-Morris) and Elovich. All these isotherms are better defined in Appendix G. The procedure that was carried out was the same described in the kinetic studies, but only for adsorption processes, that is, without the presence of light nor hydrogen peroxide.

3.3.9 Adsorption isotherms

The effect of catalyst dose on the equilibrium uptake of CV (40 mg/L) was investigated with SXQ-102 and SEM-205 concentrations of 1, 2, 4, 5, 6, 7, 8 and 9 g. The experiments were performed by placing the sands in to a beaker with CV [40 mg/L] at pH = 8. In these experiments there were not the presence of hydrogen peroxide nor irradiation. With the above different catalyst concentrations to the equilibrium uptake (24 hours) and the amount of CV adsorbed was determined using a Spectrophotometer.

The adsorption isotherms are fundamentally very decisive in the design of any adsorption system. The equilibrium relationships between adsorbent and adsorbate can be described by adsorption isotherms. In the present work, the adsorption data were analyzed with four well-known isotherm models, namely, Langmuir, Freundlich, Temkin and Dubinin-Radushkevich, adsorption isotherm models. All these isotherms are better defined in Appendix G.

The concentration of crystal violet (CV) dye in solution was measured by using a UV-Visible spectrophotometric method using a UV-Vis spectrophotometer using quartz cells of path length

1 cm at wavelength 543.9 nm, and CV concentration was determined by comparing absorbance to a calibration curve Appendix H. The maximum deviation observed was lesser than $\pm 5\%$. The amounts of CV adsorbed at equilibrium (q_e) (mg/g) were calculated from subtracting final solution concentrations from the initial concentration of the aqueous solution. The q_e was calculated by the following mass balance relationship:

$$q_e = (C_0 - C_e) \cdot \frac{V}{W} \quad (3)$$

where C_0 and C_e are the initial and equilibrium liquid-phase concentrations of CV, respectively (mg/L), V the volume of the solution (L), and W is the weight of the catalysts used (g)

4 Results and Discussion

4.1 Characterization of Sands

4.1.1 UV-Vis diffuse reflectance spectroscopy (UV- Vis DRS)

The UV-Vis diffuse reflectance spectra of the Samples magnetically enriched and powdered SXQ-102 and SEM-205 are shown in Figure 3.

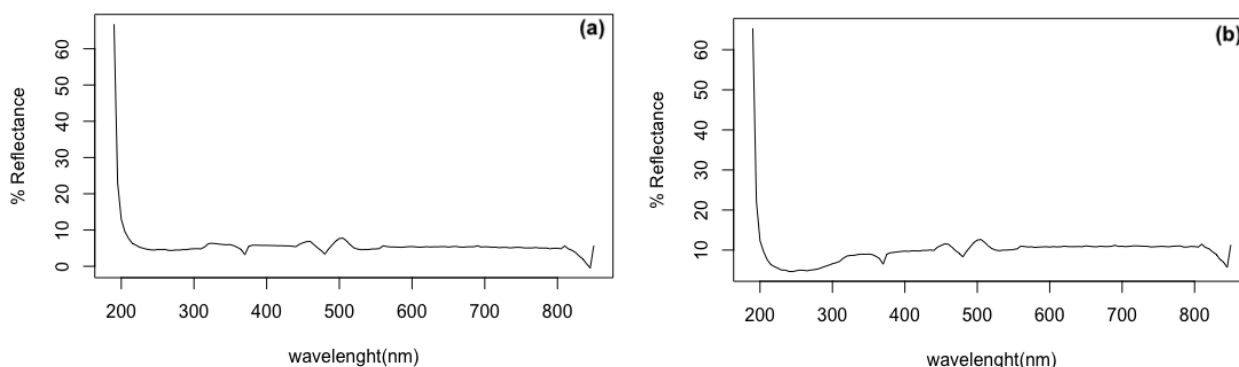


Figure 3: UV-Vis absorption spectrum for magnetically enriched and grounded black sand fractions of SXQ-102(a) and SEM-205(b).

The gap energy assessment was determined using the absorption spectrum based on the Kubelka-Munk equation (Appendix F). This equation allows to obtain the value of the band energy through the values of the function. If the value of $[F(R)h\nu]^{1/n}$ vs $h\nu$ is plotted and a straight line that crosses the axis is extrapolated of the coordinates as shown in Figures 4 .

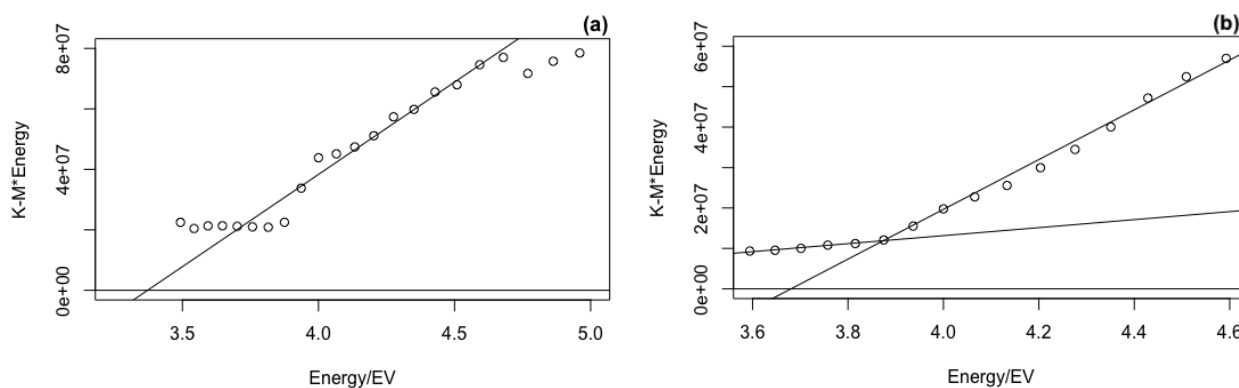


Figure 4: Tauc plot using the UV-Vis DRS of SXQ-102(a) and SEM-205(b).

Table 10: Band-gap values of the sands.

Sand	Eg	Wavelength
SXQ-102	3.37 eV	376 nm
SEM-205	3.68 eV	337 nm

4.2 Crystal Violet Dye Characterization

4.2.1 UV-Vis Spectroscopy

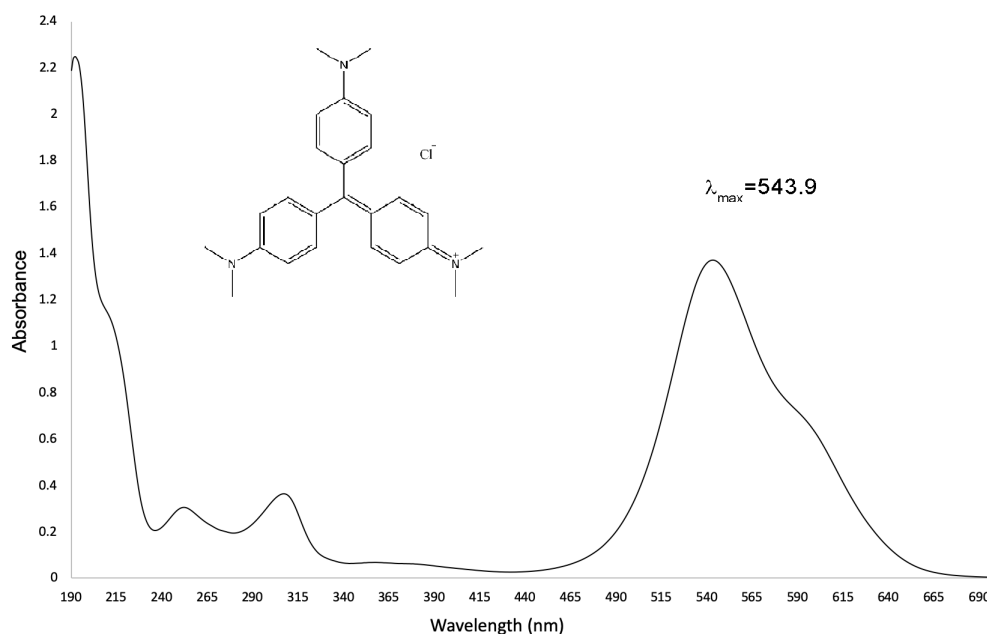


Figure 5: UV-Vis spectrum of CV dye

In Figure 5, There are 3 characteristic peaks, the most outstanding belong to the chromophore of the crystal violet dye that absorbs in maximum wavelength of 543.9 nm, there is a shoulder at 588 nm that also belongs to the chromophore of the dye and coincides with that reported by the literature [9]. The peaks that are in the range of 240 nm to 315 nm represent the aromatic rings and the C-N bonds. The shoulder in the 210 nm region could represent the chlorine cation.

4.2.2 Fourier Transform Infrared Spectrophotometry (FTIR)

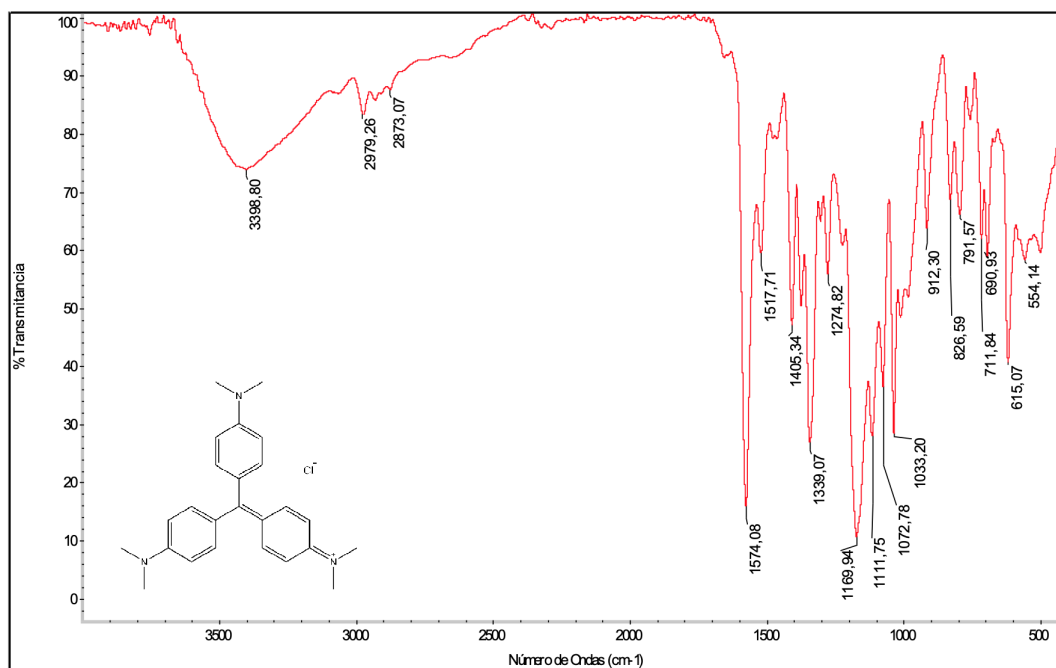


Figure 6: FTIR spectrum of CV dye.

The Figure 6 shows the FTIR spectrum. There is more than one peak obtained in the region of the C-H bending vibrations ($900\text{--}600\text{cm}^{-1}$) that can support the presence of an aromatic structure. In region $1300\text{--}1000\text{cm}^{-1}$, there is a peak at 1072cm^{-1} refers to C-H bending vibrations, and a peak at 1169.94cm^{-1} corresponds to the C-N stretching vibrations. The benzene rings are very clear supportive to the peak at 1517.71cm^{-1} that acts the C=C stretching of the benzene ring, and a peak at 2979.26cm^{-1} for C-H stretching with asymmetric CH_3 group. FTIR spectra of this dye show the presence of a band in 3398.8cm^{-1} allot to N-H stretching vibrations of primary amines. This last peak may be due to traces of trimethylmethane compounds that contain the Crystal violet dye. This dyes commercially is found as a mixture of several trimethylmethane compounds where Crystal Violet predominates (Appendix A.1) (Table 21)

4.3 Experimental Design

The results of the crystal violet dye removal according to the proposed factorial experiment design 2^4 is presented in Table 11.

Table 11: Percentage of discoloration and degradation of CV in the Runs Performed in the Experimental Design.

No.	Variables Levels				Response
	Catalyst (Sand)	pH	[H ₂ O ₂] (M)	Irradiation (nm)	% Discoloration
1	SEM-205	3	0	NO	42.3±0.5%
2	SXQ-102	3	0	NO	27.3±0.5%
3	SEM-205	8	0	NO	37.5±0.5%
4	SXQ-102	8	0	NO	15.8±0.5%
5	SEM-205	3	1	NO	82.2±0.5%
6	SXQ-102	3	1	NO	30.6±0.5%
7	SEM-205	8	1	NO	97.3±0.5%
8	SXQ-102	8	1	NO	81.7±0.5%
9	SEM-205	3	0	365	74.3±0.5%
10	SXQ-102	3	0	365	42.6±0.5%
11	SEM-205	8	0	365	50.6±0.5%
12	SXQ-102	8	0	365	36.8±0.5%
13	SEM-205	3	1	365	76.6±0.5%
14	SXQ-102	3	1	365	72.9±0.5%
15	SEM-205	8	1	365	97.6±0.5%
16	SXQ-102	8	1	365	92.6±0.5%
17	SEM-205	8	1	NO	97.2±0.5%
18	SEM-205	8	1	NO	97.0±0.5%
19	SEM-205	8	1	NO	97.1±0.5%
20	SXQ-102	8	1	NO	81.7±0.5%

21	SXQ-102	8	1	NO	81.7±0.5%
22	SXQ-102	8	1	NO	81.6±0.5%

The dye removal percentage responses were analyzed with the R Studio software to determine the main effects and interaction between them. Table 12 shows the Analysis Of the Variance (ANOVA) of the main effects and the interactions between them. Effects with a $Pr(> F)$ of less than 0.05% were considered statistically significant. The $Pr(> F)$ is an established limit where there is a 95% confidence level. Table 12 reports the analysis of variance for the removal of the crystal violet dye, showing that 4 factors and 2 interaction were statistically significant, that is, the $Pr(> F)$ is less than 0.05. The Analysis Of Variance (ANOVA) of the model yielded the following results:

Table 12: Analysis of the variance for the removal of crystal violet dye.

Factor	Df	SumSq	MeanSq	F value	Pr(>F)	
S	1	1836	1836	51.777	0.000178	***
pH	1	1786	1786	50.366	0.000194	***
P	1	7984	7984	225.113	1.4e-06	***
I	1	686	686	19.345	0.003163	**
S:pH	1	153	153	4.314	0.076426	.
S:P	1	1	1	0.022	0.887325	
pH:P	1	1909	1909	53.813	0.000158	***
S:I	1	137	137	3.869	0.089893	.
pH:I	1	133	133	3.736	0.094518	.
P:I	1	87	87	2.441	0.162170	
S:pH:P	1	45	45	1.271	0.296743	
S:pH:I	1	13	13	0.353	0.571235	
S:P:I	1	249	249	7.027	0.032901	*
pH:P:I	1	10	10	0.280	0.613060	

Residuals	7	248	35			
—						
Significa.codes: 0'****' 0.001'***' 0.01'*' 0.05'.' 0.1' ' 1						

This analysis indicates that there is a significant difference between the sands used, pH and peroxide are important factors, but more importantly, there is a strong interaction between them. The best yields are obtained when both factors are at their high level. UV radiation is a significant factor, but less important than the previous ones.

Figure 7 contains a normal quantile plot of the 4 main effects and 4 interactions. A straight line has been superimposed over the small irradiance main effect and irradiance:pH interaction. It is clear that the main effect of peroxide is very large, it appears to deviate substantially from the straight line. While the main effect of pH, Sand=(A), irradiation and interactions between, pH:peroxide have important effect in the process of integrated photocatalytic and adsorption. All the other main effects and interactions are negligible.

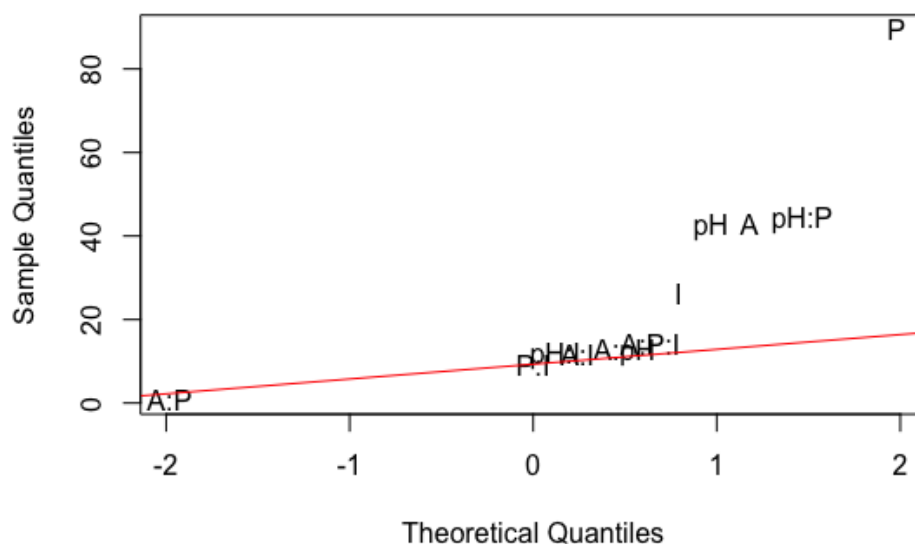


Figure 7: Q-Q plot of experimental design.

To identify possible differences between the dye reduction mechanisms that act in each arena, the design results were separated into two blocks, one for sands from Mompiche and another for sands from the slopes of Quilotoa.

Mompiche Sands. The design was reduced to 2^3 and three replicas.

Table 13: Results of discoloration percentages with SEM-205 according to the design of factorial experiments.

Mompiche Sand				
Treatments	pH	H ₂ O ₂	Irradiation	% Discoloration
1	-1	-1	-1	42.3±0.5%
2	1	-1	-1	37.5±0.5%
3	-1	1	-1	82.2±0.5%
4	1	1	-1	97.3±0.5%
5	-1	-1	1	74.3±0.5%
6	1	-1	1	50.6±0.5%
7	-1	1	1	76.6±0.5%
8	1	1	1	97.6±0.5%
9	1	1	-1	97.2±0.5%
10	1	1	-1	97.0±0.5%
11	1	1	-1	97.1±0.5%

Table 14: Analysis of the variance for the response percentage of discoloration using SEM-205 sand

Factor	Df	SumSq	MeanSq	F value	Pr(>F)	
pH	1	447	447	22.499	0.009015	**
P	1	3914	3914	197.076	0.000149	***
I	1	105	105	5.278	0.083173	.
pH:P	1	684	684	34.414	0.004216	**
pH:I	1	32	32	1.601	0.274485	
P:I	1	315	315	15.849	0.016386	*
Residuals	4	79	20			
Significa.codes: 0'****' 0.001'***' 0.01'**' 0.05'.' 0.1' ' 1						

This analysis indicates that pH and peroxide continue to be the most important factors, with a strong interaction between them. The best yields are obtained when both factors are at a high level. UV radiation is not a significant factor for Mompiche, more significant is its interaction with peroxide. It seems that in the case of Mompiche, surface adsorption is the mechanism that defines the process of dye removal.

Statistical analysis for the crystal violet dye removal response using the quantile graph showed that the concentration of hydrogen peroxide, the interaction between pH and peroxide, pH and the interaction between peroxide concentration and Irradiation as significant parameters in dye removal for the integrated photocatalytic reaction and adsorption system using black sands from Ecuador (Figure 8).

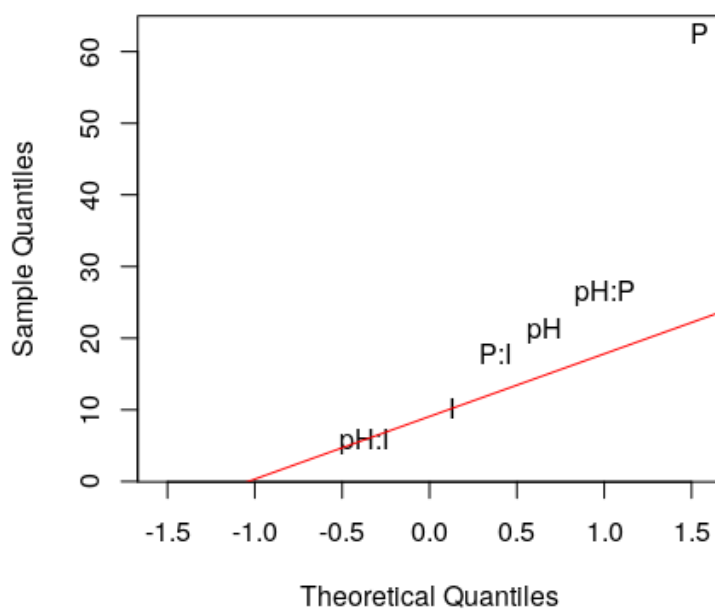


Figure 8: Q-Q plot of experimental design (SXQ-102).

For the experiment with Quilotoa the design was reduced to 2^3 and three replicas.

Table 15: Results of discoloration percentages with SXQ-102 according to the design of factorial experiments.

Quilotoa Sand				
Treatments	pH	H ₂ O ₂	Irradiation	% Discoloration
1	-1	-1	-1	27.3±0.5%
2	1	-1	-1	15.8±0.5%
3	-1	1	-1	30.6±0.5%
4	1	1	-1	81.7±0.5%
5	-1	-1	1	42.6±0.5%
6	1	-1	1	36.8±0.5%
7	-1	1	1	72.9±0.5%
8	1	1	1	92.6±0.5%
9	1	1	-1	81.7±0.5%
10	1	1	-1	81.7±0.5%
11	1	1	-1	81.6±0.5%

Table 16: Analysis of the variance for the response percentage of discoloration using SXQ-102 sand

Factor	Df	SumSq	MeanSq	F value	Pr(>F)	
pH	1	1479	1479	33.102	0.004526	**
P	1	3972	3972	88.877	0.000706	***
I	1	684	684	15.306	0.017361	*
pH:P	1	1263	1263	28.265	0.006020	**
pH:I	1	111	111	2.493	0.189528	
P:I	1	28	28	0.636	0.469884	
Residuals	4	179	45			
Significa.codes: 0'***' 0.001'***' 0.01'*' 0.05'.' 0.1' ' 1						

This analysis indicates that pH and peroxide continue to be the most important factors, with a strong interaction between them. The best yields are obtained when both factors are at a high level. UV radiation is a significant factor for Quilotoa. It seems that in the case of Quilotoa a photocatalysis mechanism is present during the dye removal process.

Figure 9 contains a normal quantile plot of the 3 main effects and 3 interactions for SXQ-102. A straight line has been superimposed over the small irradiance main effect and irradiance:pH interaction. The main effect of peroxide is very large. While the main effect of pH, Irradiation and interactions between pH:peroxide significant in the integrated photocatalytic adsorption process with SXQ-102. All the other main effects and interactions are negligible. It seems that in SXQ-102 predominate an photocatalytic process.

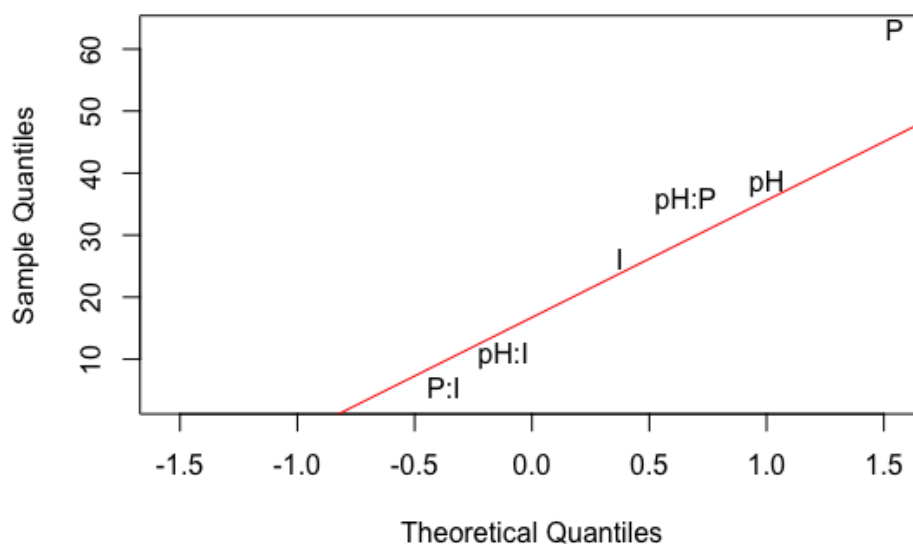


Figure 9: Q-Q plot of experimental design (SEM-205).

4.4 Kinetics of IPCA and Adsorption with SXQ-102 and SEM-205

4.4.1 Kinetics with SXQ-102 of best results of IPCA and adsorption processes.

Table 17: Best results of IPCA and adsorption processes with SXQ-102 obtained from experimental design

Run	Variables Levels				Result
No	Catalyst (Sand)	pH	H ₂ O ₂ (M)	Irradiation (nm)	%Discoloration
4	SXQ-102	8	0	NO	17.4±0.5%
16	SXQ-102	8	1M	365nm	93.7±0.5%

The kinetics of the best results obtained for adsorption and integrated photocatalysis and adsorption was performed with the aim of comparing them. Figure 10 shows the kinetic of both processes with Quilotoa sand (SXQ-102). The red line corresponds to the adsorption process without the presence of light nor peroxide. The black line represents the integrated photocatalysis and adsorption process. The adsorption process shows that in 2 hours it removal 17.4%. The kinetics of the integrated photocatalysis and adsorption process shows that degrades exponentially reaching 93.7% removal in 2 hours.

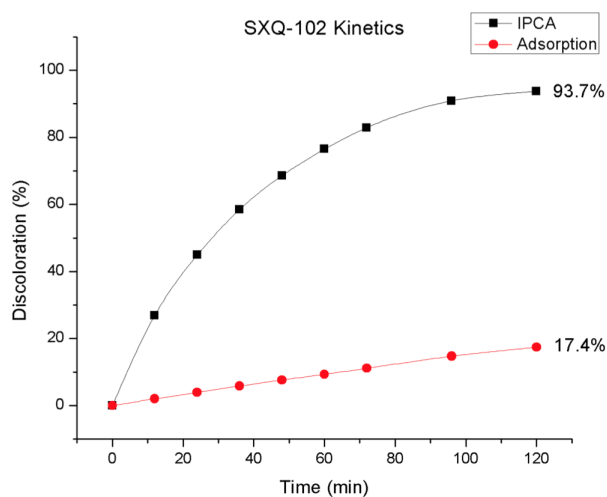


Figure 10: Kinetics for SXQ-102 IPCA and Adsorption.

In the Figure 11 we can see before and after the dye when treated by integrated photocatal-

ysis and adsorption process.



Figure 11: CV dye in solution and Discoloration by SXQ-102 after 2 hours.

4.4.2 Kinetics with SEM-205 of best results of IPCA and adsorption processes.

Table 18: Best results of IPCA and adsorption processes with SEM-205 obtained from experimental design

Run	Variables Levels				Result
No	Catalyst (Sand)	pH	H ₂ O ₂ (M)	Irradiation (nm)	%Discoloration
3	SEM-205	8	0	NO	37.6±0.5%
15	SEM-205	8	1M	±0.5 365 nm	97.1%

The kinetics of the best results obtained for adsorption and integrated photocatalysis and adsorption was performed with the aim of comparing them. Figure 12 shows the kinetic of both processes with Mompiche sand (SEM-205). The red line corresponds to the adsorption process without the presence of light nor peroxide. The black line represents the integrated photocatalysis and adsorption process. The adsorption process shows that in 2 hours it removal 37.6%. The kinetics of the integrated photocatalysis and adsorption process shows that degrades exponentially reaching 97.1% removal in 2 hours and more that 90% in less than 1 hour.

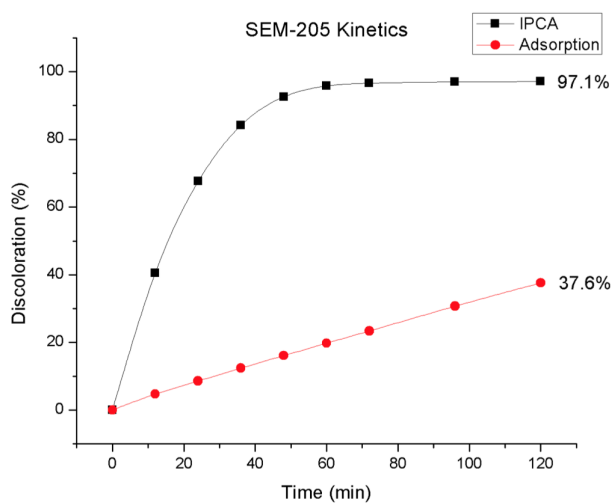


Figure 12: Kinetics for SEM-205 IPCA and Adsorption.

In the Figure 13 we can see before and after the dye when treated by integrated photocatalysis and adsorption process.

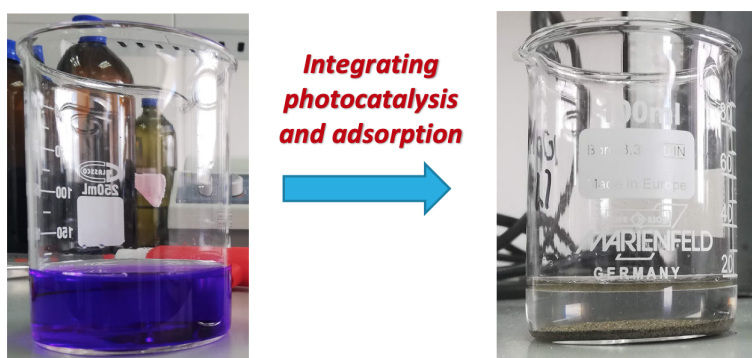


Figure 13: CV dye in solution and Discoloration by SXQ-102 after 2 hours.

It is clear that integrating photocatalysis process to the adsorption process we greatly improve the removal process, with these results confirmed that the sands can be used as photocatalytic adsorbents. Mompiche shows better result due to their adsorbent nature also because it's particle size is smaller than Quilotoa, which increase its surface area and then improves the process.

4.5 UVVis absorption spectra

In order to monitor the removal of the crystal violet dye under adsorption conditions and IPCA, adsorption spectra were made at different levels. As shown in Figures 14 and 15, the initial solution shows 4 characteristic peaks located at 215 nm, 250 nm, a small peak at 310 nm and 543 nm with a shoulder at 588 nm, attributed to the chromophore group and benzene rings of the violet crystal molecule.

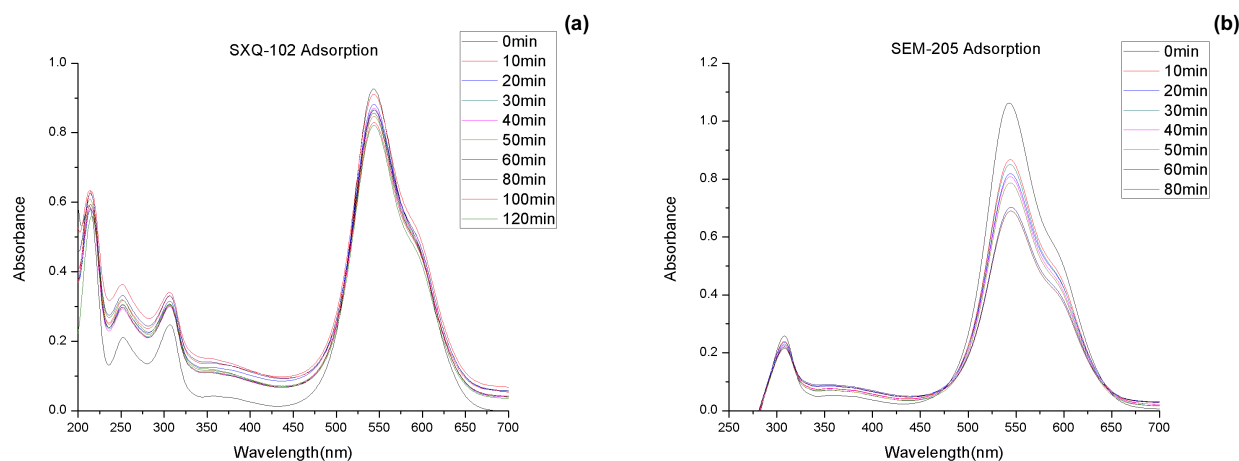


Figure 14: Absorption spectra of the initial CV solution and after 10, 20, 30, 40, 50, 60, 70, 80, 100, 120 min. Conditions: $[CV]_0=40$ ppm, $pH=8$, Sand= SXQ-102(a) and SEM-205(b). (Adsorption)

The spectrum observed after adsorption of the dye with SXQ-102 (Figure 14 (a)) exhibits a smaller decrease of the 4 characteristic peaks, as mentioned in the previous section, with this process only 17% discoloration was achieved.

In figure 14 part (b) the spectrum is shown after adsorption of the dye with SEM-205, in this case, a notable decrease is shown in the 4 characteristic peaks but not 100% with this process a 38% discoloration was achieved. With these results, we can conclude that both arenas are absorbent but not very effective.

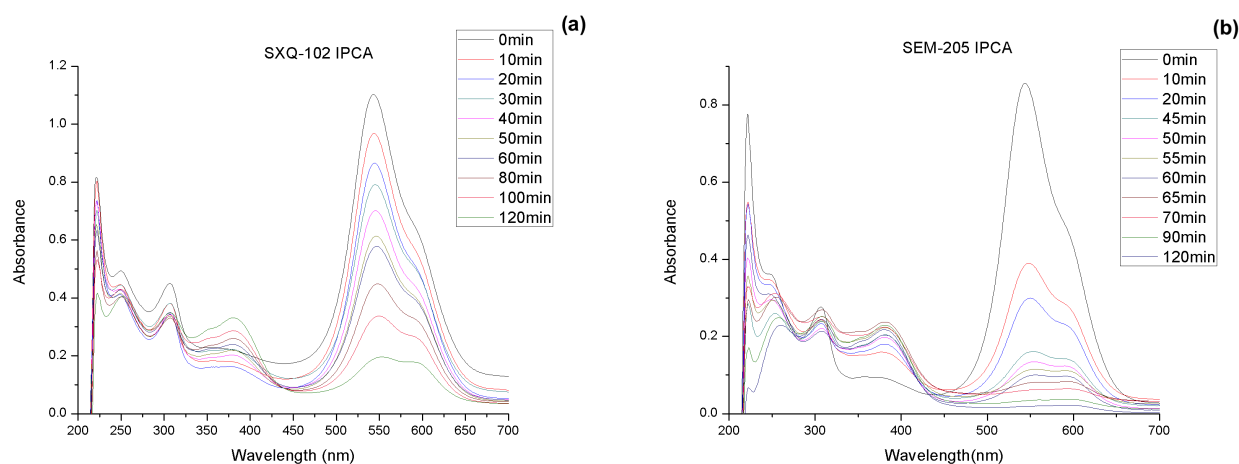


Figure 15: Absorption spectra of the initial CV solution and after 10, 20, 30, 40, 50, 60, 70, 80, 100, 120 min. Conditions: $[CV]_0=40$ ppm, $pH=8$, $[H_2O_2]$, Irradiation, Sand= SXQ-102(a) and SEM-205(b). (Integrated Photocatalysis and Adsorption (IPCA))

Figure 15 shows full instantaneous UV-Vis adsorption spectra of the reaction mixture for both sands, registered at different times. At $t=0$ the spectra presents a main band at 543.9 nm, a shoulder at 590 nm and some minor peaks in the UV region at 215, 250 and 543 nm. It can be noticed that these bands keep decreasing while the reaction is advances and by the other hand, the signal at 310 nm is growing. That seems to suggesst the apparition of by-products .

In the last spectrum after the IPCA process with SEM-205 (figure 15 (b)), a significant decrease in the peak at 543 nm is observed, the decrease in this peak almost disappears completely. With this sand a 97% discoloration was achieved.

4.6 Adsorption Isotherms

The adsorbent dose represents an important parameter for the study of isotherm models. The effect of adsorbent dose on the amount of CV adsorbed was conducted over a range of SEM-205 and SXQ-102 doses of 1 to 9 g /15 mL at an initial concentration of the dye (40 mg/L) for a contact time of 24 hours at constant pH 8.0, and the results are presented in Figure 16. It is clearly observed that with increasing the adsorbent dose from 1 to 9g, the percentage of discoloration of CV was increased from 47 to 79% at 40 mg/L of the dye concentration and with SEM-205 sand and for SXQ-102 there was an increase of 6 to 31% at the same conditions. The increase in percentage removal with the adsorbent dose can be attributed to the increase of the available adsorption surface and availability of more adsorption sites.

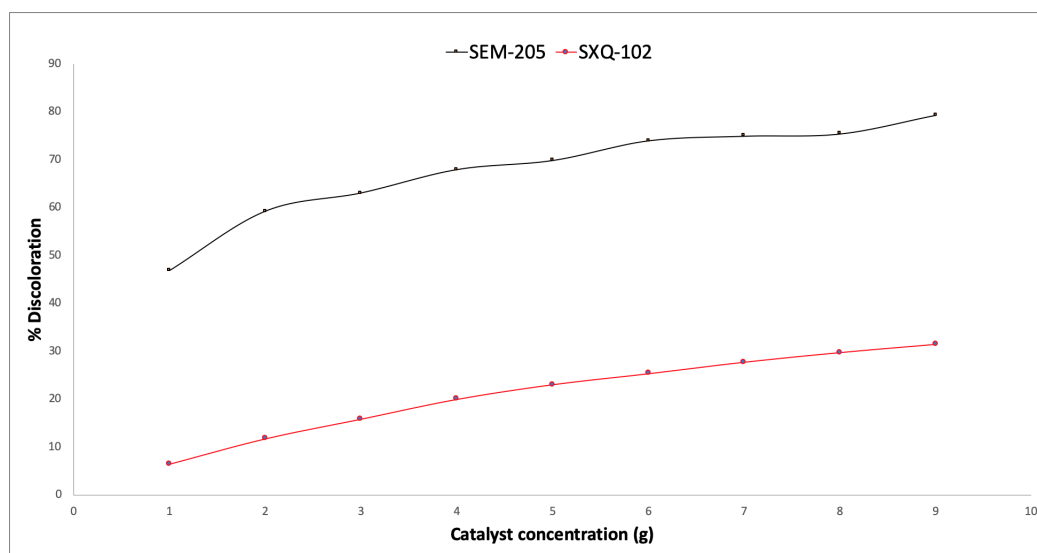


Figure 16: Relation between amounts of CV adsorbed at equilibrium (q_e) using different concentrations of SXQ-102 and SEM-205

Adsorption is typically represented through isotherms, that is, the quantity of adsorbate on the adsorbent as a function of its pressure (in case of gas) or concentration (in case of liquid) at a constant temperature. Amount of adsorbate is almost continuously normalized by the mass of the adsorbent to permit comparison of various material. Equilibrium studies on adsorption process provide data on the capacity of the adsorbent.

Adsorption isotherms is a representation of the equilibrium adsorption capacity. q_e [mg/g] measured at at different concentration plotted as a function of the equilibrium concentration

($C_e[mg/L]$) of solution studied.

The equilibrium experiment data were analysed by different models Langmuir, Freundlich, Temkin and Dubinin-Radushkevich.

Table 19 shows the data obtained from isotherm models.

Table 19: Isotherm models obtained from linear solvation

Isotherm models	Parameters	SEM-205	SXQ-102
Langmuir	$q_m(mg/g)$	24.77 \pm 1.98	52.93 \pm 2.42
	$K_L(L/mg)$	13.93 \pm 1.4	44.03 \pm 2.86
	R_L	1.78E-3 \pm 1.88E-4	5.67E-4 \pm 3.68E-5
	R^2	0.96	0.98
	Error	1.01E-4	1.72E-6
	Fvalue	204.95	475,78
Freundlich	n	2.19 \pm 0.12	2.02 \pm 0.06
	$K_F(mg^{1-1/n}L^{1/n}/g)$	40.04 \pm 2.40	170.70 \pm 10.24
	R^2	0.98	0.99
	Error	2.6E-3	1.16E-4
	Fvalue	317.71	995.06
Temkin	$\beta(J/mol)$	6.22 \pm 0.35	13.70 \pm 0.67
	b	0.40 \pm 0.02	0.18 \pm 8.80E-3
	$K_T(L/g)$	101.49 \pm 30.45	303.90 \pm 100.61
	R^2	0.97	0.98
	Error	2.09	1,11
	Fvalue	309.53	421.99
Dubinin-Radushkevich	$q_m(mg/g)$	25.56 \pm 1.19	70.19 \pm 2.67
	K	0.02 \pm 9.9E-4	0.01 \pm 4.33E-4
	E	5.55 \pm 0.17	6.80 \pm 0.14
	R^2	0.97	0.99
	Error	0.01	9.47E-4
	Fvalue	268.18	641.57

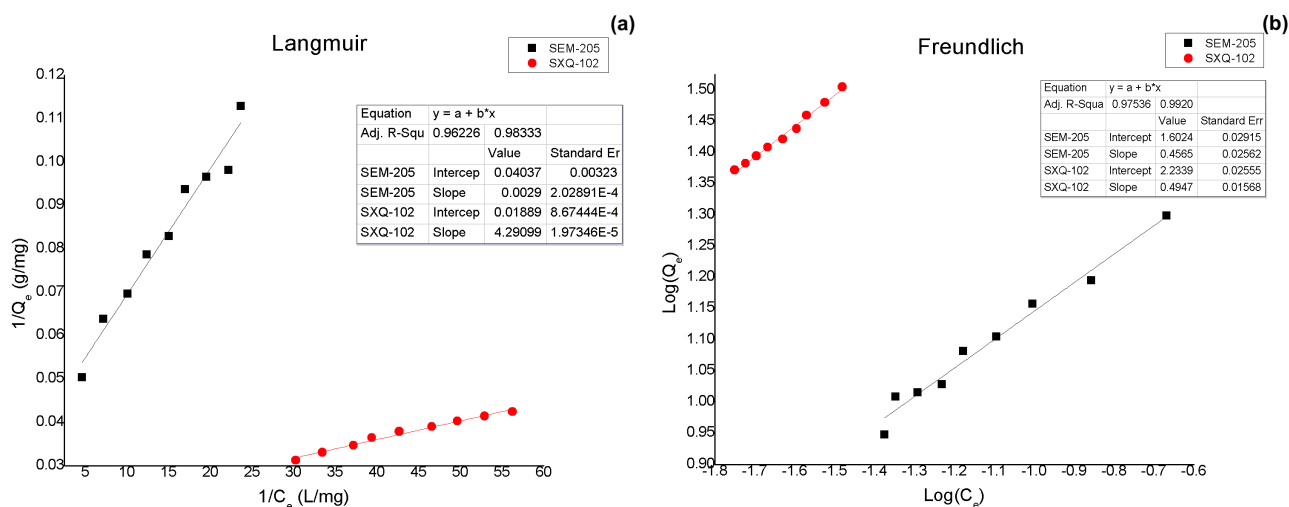
The theoretical **Langmuir** sorption isotherm

Figure 17: Linear Langmuir (a) and Freundlich (b) model for adsorption of Crystal Violet over SEM-205 and SXQ-102.

Is the most widely used for the adsorption of a pollutant from a liquid solution. It is valid for adsorption of a solute from a liquid solution as monolayer adsorption on specific homogenous sites (a finite number of identical sites) within the adsorbent surface, which are energetically equivalent. Therefore, the Langmuir isotherm model estimates the maximum adsorption capacity produced from complete monolayer coverage on the adsorbent surface (Appendix G.1.0.1). The results obtained from Langmuir model for the removal of crystal violet dye by SEM-205 and SXQ-102 have coefficients of determination of $R^2 = 0.96$ and 0.98 respectively (Table 19). Figures 17 part (a) shows the isotherm plot and the experimental data of Langmuir isotherms. This figure indicates the applicability of Langmuir isotherm model. The maximum monolayer capacity Q_m obtained from linear solvation of Langmuir model for SXQ-102 and SEM-205 are 24.77 ± 1.98 mg/g and 52.93 ± 2.42 mg/g, respectively.

The Freundlich isotherm

Model is applicable to the adsorption on heterogeneous surfaces with interaction between adsorbed molecules. It also suggests that sorption energy exponentially decreases on completion of the sorption centers of an adsorbent. Therefore, Freundlich isotherm can be employed to describe the heterogeneous systems. K_F represents the quantity of dye adsorbed onto adsorbent for unit equilibrium concentration. The n value indicates the degree of non-linearity

between solution concentration and adsorption as follows: if the value of $n = 1$, the adsorption is linear; $n < 1$, the adsorption process is chemical; if $n > 1$, the adsorption is a favorable physical process (Appendix G.1.0.2).

Figure 17 part (b) represents the plot of $\log(C_e)$ versus $\log(Q_e)$ with the intercept value of $\log(K_F)$ and the slope of $1/n$. The coefficients of determination for SEM-205 and SXQ-102 are $R^2 = 0.98$ and 0.99 , respectively. This result indicates that the experimental data fitted Freundlich model is better than Langmuir in both cases and the $n > 1$, indicating that adsorption of CV onto SEM-205 and SXQ-102 are physical process.

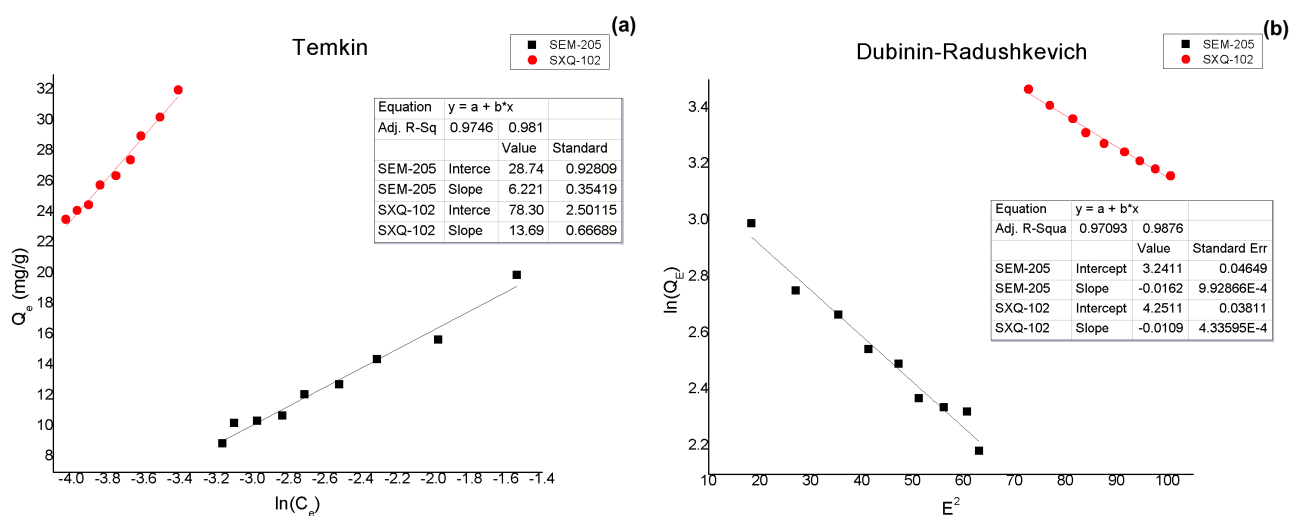


Figure 18: Linear Temkin (a) and Dubinin-Radushkevich (b) model for adsorption of Crystal Violet over SEM-205 and SXQ-102.

Temkin isotherm

Model assumes that the heat of adsorption of all the molecules in the layer decreases linearly with coverage due to adsorbate-adsorbent interactions as well as the adsorption is characterized by a uniform distribution of maximum binding energy. The derivation of the Temkin isotherm assumes that the fall in the heat of sorption is linear rather than logarithmic, as implied in the Freundlich equation (Appendix G.1.0.3). Figure 18 part (a) shows the adsorption data according to the linear form of the Temkin isotherm equation and value of constants and coefficients are given in Table 19. The coefficients of determination obtained for SEM-205 and SXQ-102 are $R^2 = 0.97$ and 0.98 , respectively, which indicates that the Temkin isotherm fit well the equilibrium data obtained for the adsorption of CV onto SEM-205 and SXQ-102. The

values of b indicate that the both processes are exothermic.

Dubinin-Radushkevich (D-R) isotherm

Model does not assume a homogeneous surface or constant sorption potential. It was applied to estimate the porosity apparent free energy and the characteristic of adsorption and it has commonly been applied in the form equation and its linear form (Appendix G.1.0.4). Figure 18 part (b) shows the plot of $\ln(Q_e)$ versus (ε^2) of the experimental data for the adsorption of CV onto SEM-205 and SXQ-102. The slope gives $K(\text{mol}^2(\text{kJ}^2)^{-1})$ and the intercept yields the adsorption capacity, Q_m (mg/g). The mean free energy of adsorption (E), defined as the free energy change when one mole of ion is transferred from infinity in solution to the surface of the sorbent. Calculated D-R constants for the adsorption of CV on SEM-205 and SXQ-102 are shown in Table 19; the values of coefficients of determination are $R^2 = 0.97$ and 0.98 , respectively which indicating that the D-R fit well the experimental data in comparable with the Langmuir and Temkin isotherm models. The maximum capacity Q_m obtained using D-R isotherm model for adsorption of CV on SEM-205 and SXQ-102 are 25.53 and 70.1 mg/g, respectively (Table 19). The values of E is 5.55 ± 0.17 KJ/mol for SEM-205 and 6.80 ± 0.14 KJ/mol for SXQ-102 sand. The typical range of bonding energy for ion-exchange mechanisms is 8-16 KJ/mol, indicating that physisorption plays a significant role in the adsorption process of CV onto SEM-205 and SXQ-120.

Parameters related to each isotherm were determined by using linear regression analysis and the square of the correlation coefficients (R^2) have been calculated. A list of the parameters obtained together with R^2 values is given in Table 19. A comparison of the experimental isotherms with the adsorption isotherm models showed that the Freundlich isotherm represent the best fit of experimental data for both sands SEM-205 and SXQ-102 as compared to the other isotherm equations ($R^2 = 0.97$ and 0.99), respectively. The maximum monolayer capacity obtained for CV adsorption on SEM-205 and SXQ-102 were 24.771.08 mg/g and 52,932.42 mg/g.

4.7 Kinetic Study

Several models were used to examine the rate controlling of the adsorption process such as chemical reaction, diffusion control and mass transfer. Since the kinetic parameters are helpful

for the prediction of adsorption rate and give important information for designing and modeling the adsorption processes, the kinetics of the adsorption of CV onto SEM-205 and SXQ-102 were investigated. Therefore, pseudo first-order, pseudo second-order, Elovich and intraparticle diffusion kinetic models were applied for the adsorption of CV on SEM-205 and SXQ-102 and the conformity between experimental data and the model-predicted values were expressed by the coefficients of determination (R^2).

Table 20: Comparison of kinetic models

Kinetic models	Parameters	SEM-205 Ads	SXQ-102 Ads
Pseudo-First Order	$k_1(\text{min}^{-1})$	$1.52\text{E-}5 \pm 1.31\text{E-}6$	$2.92\text{E-}6 \pm 5.53\text{E-}8$
	$q_e \text{exp}(\text{mg/g})$	27.77 ± 1.98	52.93 ± 2.42
	$q_e \text{cal}(\text{mg/g})$	$24.24 \pm 2.04\text{E-}3$	$52.93 \pm 1.8\text{E-}4$
	R^2	0.95	0.99
	<i>Error</i>	$1.45\text{E-}7$	$2.63\text{E-}10$
	<i>Fvalue</i>	139.28	2736.13
Pseudo-Second Order	$k_2(\text{g/mgmin})$	$1.72\text{E-}6 \pm 3.12\text{E-}7$	$6.35\text{E-}8 \pm 5.82\text{E-}9$
	$q_e \text{exp}(\text{mg/g})$	24.77 ± 1.98	52.93 ± 2.42
	$q_e \text{cal}(\text{mg/g})$	24.23 ± 3.67	52.77 ± 2.43
	h	0.0099	0.00017
	R^2	0.92	0.93
	<i>Error</i>	110019.28	31367.25
Elovich	$\alpha(\text{mg/gmin})$	$1.64\text{E-}3 \pm 3.29\text{E-}4$	$4.53\text{E-}4 \pm 9.06\text{E-}5$
	$\beta(\text{g/mg})$	45.99 ± 1.84	97.64 ± 6.83
	R^2	0.99	0.98
	<i>Error</i>	$2.97\text{E-}6$	$2.02\text{E-}6$
	<i>Fvalue</i>	624.59	203.94
Weber-Morris	$k_{id}(\text{mgmin}^{1/2}/\text{g})$	$0.005 \pm 1.084\text{E-}4$	$0.002 \pm 8.996\text{E-}5$
	C	$-0.008 \pm 8.750\text{E-}4$	$-0.008 \pm 7.260\text{E-}4$
	R^2	0.99	0.99
	<i>Error</i>	$1.57\text{E-}6$	$1.08\text{E-}6$
	<i>Fvalue</i>	2276.34	694.30

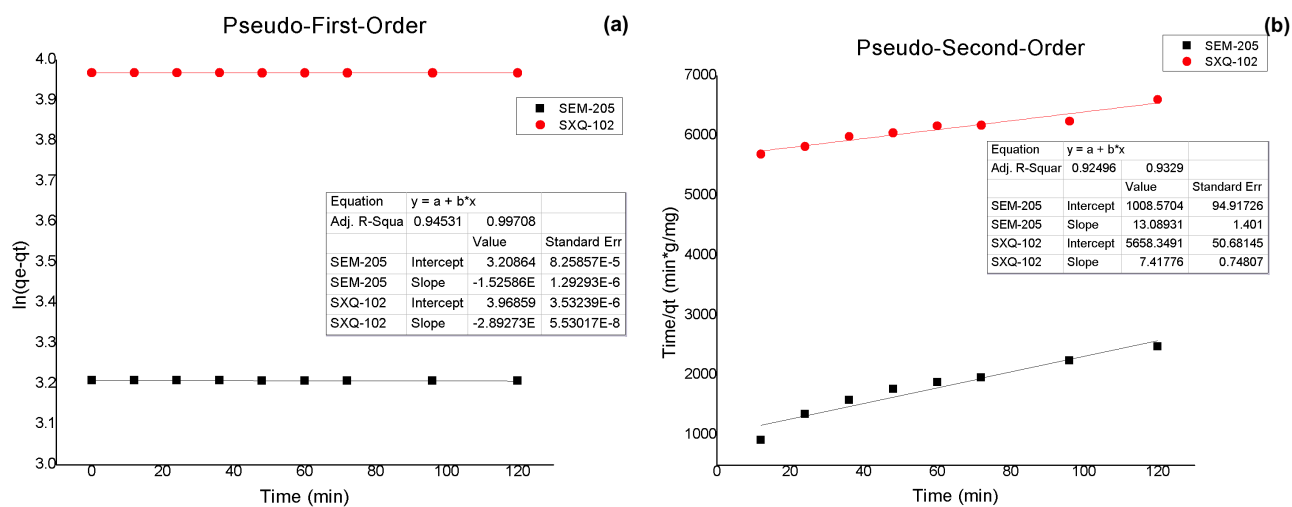


Figure 19: Pseudo-First-order (a) and Pseudo-second-order model (b) for removal of crystal violet dye by SEM-205 and SXQ-102.

The rate constant of adsorption is determined from the pseudo-first-order model, the earliest known equation describing the adsorption rate based on the adsorption capacity (Appendix G.2.0.1). Figure 19 part (a) represents plot the values of $\text{Log}(q_e - q_t)$ versus t of the pseudo-first-order model and the parameters, k_1 and q_e , were calculated from the slope and intercept. If the calculated q_e does not equal the experimental q_e then the reaction is not likely to be the first-order reaction, but in this case, for SXQ-102 and SEM-205 the values of $q_{e,exq}$ are highly similar to $q_{e,cal}$. Even this plot has a high coefficient of determination with the experimental data for SXQ-102 and SEM-205 and low standard error values. Therefore the adsorption of CV onto SXQ-102 and SEM-205 are first-order reactions.

Figure 19 part (b) shows the pseudo-second-order model results, for SXQ-102 and SEM-205 the values of $q_{e,exq}$ are highly similar to $q_{e,cal}$. This plot has a high coefficient of determination with the experimental data for SXQ-102 and SEM-205, but high standard error values. Therefore the adsorption of CV onto SXQ-102 and SEM-205 does not follow a pseudo-second-order model (Appendix G.2.0.2).

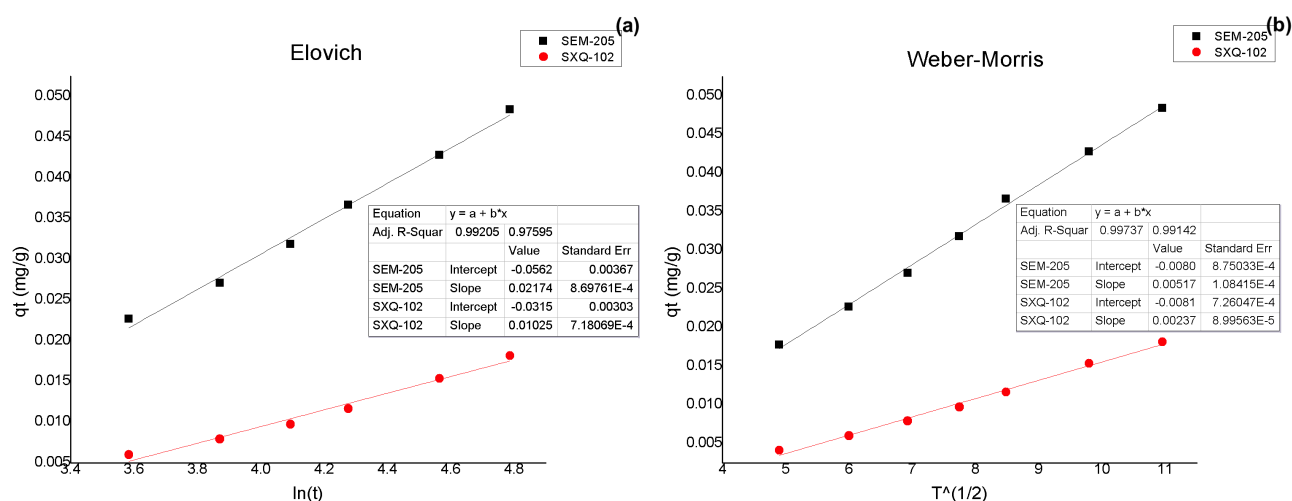


Figure 20: Elovich (a) and Weber-Morris model (b) for removal of crystal violet dye by SEM-205 and SXQ-102.

Elovich equation is a rate equation based on the adsorption capacity (Appendix G.2.0.3). Figure 20 part (a) shows plot of q_t versus $\ln(t)$ and the Elovich constants were calculated from the slope ($1/\beta$) and intercept $(1/\beta)\ln(\alpha \cdot \beta)$ of the straight lines and reported in Table 20. The coefficients of determination R^2 are 0.99 and 0.98 for SEM-205 and SXQ-102, respectively without definite role, which reflects the applicability of this model to the experimental data obtained for the adsorption of CV on SEM-205 and SXQ-102.

The dye adsorption is usually controlled by either the intraparticle or the liquid-phase mass transport rates. If the experiment is a batch system with rapid stirring, there is a possibility that intraparticle diffusion (Weber-Morris) is the rate controlling step. This possibility was tested in terms of a graphical relationship between q_t and the square root of time, $t^{1/2}$, according to the intraparticle diffusion model proposed by Weber and Morris (Appendix G.2.0.4). Since the Crystal Violet dye is probably transported from its aqueous solution to the SEM-205 or SXQ-102 by intraparticle diffusion, so the intraparticle diffusion is another kinetic model should be used to study the rate-limiting step for crystal violet adsorption onto SEM-205 and SXQ-102. If the intraparticle diffusion is involved in the adsorption process, then the plot of q_t versus $t^{1/2}$ would result in a linear relationship, and the intraparticle diffusion would be the controlling step if this line passed through the origin.

The shape of Figure 20 part (b) confirms straight lines not passed through the origin with coefficients of determination ranged from low to high value without definite meaning, which is

indicative of some degree of boundary layer control and this further shows that the intraparticle diffusion is not only the rate controlling step for the adsorption of the crystal violet on SEM-205 and SXQ-102 , but also other processes may control the rate of adsorption. The intraparticle diffusion rate constant, K_{id} , were $0.005 \pm 1.084E-4$ ($\text{mg} \cdot \text{min}^{1/2}/\text{g}$) for process with SEM-205 and $0.002 \pm 8.996E-5$ ($\text{mg} \cdot \text{min}^{1/2}/\text{g}$) for process with SXQ-102.

5 Conclusions

- Sands from Mompiche and Quilotoa were successfully utilized as a low cost alternative photocatalytic adsorbent for the removal of crystal violet dye, being Mompiche more effective.
- The best conditions for degradation of the crystal violet dye were found using an experimental design.
- The influence of four reaction factors was determined: hydrogen peroxide concentration, irradiation, pH and catalyst, on the removal of the crystal violet dye using black sands from the equator with photocatalytic absorbers. The best conditions of the integrated photocatalysis and adsorption process using Ecuadorian sands were 5 g of catalyst, 1M hydrogen peroxide concentration, pH: 8 and irradiation time: 2 hours.
- The technical feasibility of the removal of the crystal violet dye in water was evaluated using black sands from the equator as photocatalytic absorbers, the comparative study showed that the removal activity of Mompiche sands (SEM-105) was better than that of Quilotoa (SXQ -102) with 97% discoloration in 2 hours compared to Quilotoa with 93%.
- Kinematics was performed with both sands where 90% discoloration is obtained in less than an hour with Mompiche.
- The adsorption isotherm study showed that the adsorption with SEM-205 followed a Freundlich model with high coefficient of determination (R^2) and a low standard error value. The maximum adsorption capacity obtained was 24.77 ± 1.98 mg/g.
- In the case of adsorption with SXQ-102, it followed the Freundlich and Dubinin-Radushkevich models with high coefficients of determination (R^2) and a low standard error value. The maximum adsorption capacity obtained was 52.93 ± 2.42 mg/g.
- Temkin and Dubinin-Radushkevish models showed that in both processes, adsorption with SEM-205 and with SXQ-102 physisorption plays a significant role in the process of removal of CV with SEM-205 and SXQ-102, and both processes are exothermic

- The adsorption kinetic data with SEM-205 and SXQ-102 are well represented by the pseudo-first-order model, with high regression coefficients and a low standard error value.

6 Recommendations

- According to the previous conclusions, it is necessary to identify the by-products formed in the integrated photocatalytic and adsorption process with SXQ-102 and SEM-205. Also, it is necessary to evaluate the photocatalytic activity and integrated adsorption of magnetic fractions of both sands under conditions of real wastewater with concentrations of different organic compounds and to quantify in addition to the removal of the presence of other residual gases. Besides, experimentation in a pilot plant reactor could be beneficial considering the number of cycles the sand can withstand.

References

- [1] WWAP (Programa Mundial de Evaluación de los Recursos Hídricos de la UNESCO). Informe Mundial de las Naciones Unidas sobre el Desarrollo de los Recursos Hídricos 2019: No dejar a nadie atrás. París, *UNESCO*. **2019**.
- [2] INEC. Medición de Los Indicadores ODS de Agua, Saneamiento e Higiene (ASH) En El Ecuador. *Inst. Nac. Estadística y Censos*. **2016**, 1–27.
- [3] Brañez, M.; Gutierrez, R.; Perez, R.; Uribe, C.; Valle, P. Pollution of Aquatic Environments Generated by Textile Industry. *Esc. Univ. Posgrado UNFV, Lima - Perú* **2018**, V.XXIII, 129–144.
- [4] Asociación de Industrias Textiles del Ecuador (AITE). La industria textil apuesta e invierte en el Ecuador. Quito. Ecuador: *Boletín Mensual AITE*. **2010**.
- [5] Instituto Nacional de Estadísticas y Censos (INEC). Infoeconomía Quito. Ecuador. INEC. **2012**.
- [6] Instituto Nacional de Estadísticas y Censos (INEC). Estadísticas de Gasto Empresarial en Protección Ambiental. Quito. Ecuador. *INEC*. **2006**.
- [7] Tinoco Gómez, O. R.; Medina Escudero, A. M.; Zapata Gamarra, H. Tratamiento de Efluentes Textiles Con Luz Ultravioleta Solar. *Ind. Data* **2014**, 14 (2), 009.
- [8] Fan, H.; Huang, S.; Chung, W.; Jan, J.; Lin, W.; Chen, C. Degradation Pathways of Crystal Violet by Fenton and Fenton-like Systems : Condition Optimization and Intermediate Separation and Identification. *J. Hazard. Mater* **2009**, 171, 1032–1044.
- [9] Au, W.; Pathak, S.; Collie, C. J.; Hsu, T. C. Cytogenetic Toxicity of Gentian Violet and Crystal Violet on Mammalian Cells in Vitro. *Mutat. Res. Toxicol.* **1978**, 58 (2–3), 269–276.
- [10] Mani, S.; Bharagava, R. N. Exposure to Crystal Violet, Its Toxic, Genotoxic and Carcinogenic Effects on Environment and Its Degradation and Detoxification for Environmental Safety; **2016**; Vol. 237.

- [11] T.A. Saleh, Isotherm, kinetic, and thermodynamic studies on Hg (II) adsorption from aqueous solution by silica-multiwall carbon nanotubes, *Environ. Sci. Pollut. Res.* **2015**, 22 (21). 16721–16731.
- [12] T.A. Saleh, Simultaneous adsorptive desulfurization of diesel fuel over bimetallic nanoparticles loaded on activated carbon, *J. Clean. Prod.* **2018**, 172. 2123–2132.
- [13] Abbas F. S. Dye removal from wastewater using agricultural waste. *Advances in Environmental Biology*, **2013**, 6, 1019-1026.
- [14] Q. Zhu, et al., Adsorption of pyridine from aqueous solutions by polymeric adsorbents MN 200 and MN 500. Part 1: adsorption performance and PFG-NMR studies, *Chem. Eng. J.* **2016**, 306, 67–76.
- [15] A. Rahman, T. Urabe, N. Kishimoto, Color removal of reactive procion dyes by Clay adsorbents, *Proc. Environ. Sci.* **2013**, 17, 270–278.
- [16] U. Pal, et al., Mixed titanium, silicon, and aluminum oxide nanostructures as novel adsorbent for removal of rhodamine 6G and methylene blue as cationic dyes from aqueous solution, *Chemosphere* **2016**, 163, 142–152.
- [17] A. Rossner, S.A. Snyder, D.R.U. Knappe, Removal of emerging contaminants of concern by alternative adsorbents, *Water Res* **2009**, 43 (15), 3787–3796.
- [18] N.F. Zainudin, A.Z. Abdullah, A.R. Mohamed, Characteristics of supported nano-TiO₂/ZSM-5/silica gel (SNTZS): photocatalytic degradation of phenol, *J. Hazard. Mater.* **2010**, 174 (1–3). 299–306. A.N.
- [19] Ökte, Ö. Yılmaz, Characteristics of lanthanum loaded TiO₂-ZSM-5 photocatalysts: decolorization and degradation processes of methyl orange, *Appl. Catal. A* **2009**, 354 (1–2). 132–142.
- [20] Yahya, N.; Aziz, F.; Jamaludin, N. A.; Mutalib, M. A.; Ismail, A. F.; Salleh, W. N.; Jaafar, J.; Yusof, N.; Ludin, N. A. A Review of Integrated Photocatalyst Adsorbents for Wastewater Treatment. *J. Environ. Chem. Eng.* **2018**, 6 (6), 7411–7425.

- [21] Mutalib, M. A.; Aziz, F.; Jamaludin, N. A.; Yahya, N.; Ismail, A. F.; Mohamed, M. A.; Yusop, M. Z. M.; Salleh, W. N. W.; Jaafar, J.; Yusof, N. Enhancement in Photocatalytic Degradation of Methylene Blue by LaFeO₃-GO Integrated Photocatalyst-Adsorbents under Visible Light Irradiation. *Korean J. Chem. Eng.* **2018**.
- [22] Solar Yahya, N.; Aziz, F.; Jamaludin, N. A.; Mutalib, M. A.; Ismail, A. F.; Salleh, W. N.; Jaafar, J.; Yusof, N.; Ludin, N. A. A Review of Integrated Photocatalyst Adsorbents for Wastewater Treatment. *J. Environ. Chem. Eng.* **2018**, 6 (6), 7411–7425.
- [23] Abd El Aal, S. A.; Abdelhady, A. M.; Mansour, N. A.; Hassan, N. M.; Elbaz, F.; Elmaghraby, E. K. Physical and Chemical Characteristics of Hematite Nanoparticles Prepared Using Microwave-Assisted Synthesis and Its Application as Adsorbent for Cu, Ni, Co, Cd and Pb from Aqueous Solution. *Mater. Chem. Phys.* **2019**, 235 (June), 121771.
- [24] Badu, N., Vasumathi, N. y Bhima Rao, R. Recovery of ilmenite and other heavy minerals from teri sands (red sands) of Tamil Nadu, India. *Journal of Minerals Materials characterization Engineering.* **2009**.
- [25] Cañas-martínez, D. M.; Gauthier, H.; Pedraza-avella, J. A. Methyl Orange as a Probe Molecule. **2019**, 30–33.
- [26] Rauf, M. A.; Shehadi, I. A.; Hassan, W. W. Studies on the Removal of Neutral Red on Sand from Aqueous Solution and Its Kinetic Behavior. *Dye. Pigment.* **2007**, 75 (3), 723–726.
- [27] Perez, S. M.; Sharadqah, S. Successive Methods for the Separation of Titanium Oxide from the Black Sands of Ecuador. *J. Ecol. Eng.* **2018**, 186–190.
- [28] Perez S. and Sharadqah S. Recovery of TiO₂ from titaniferous sand of Esmeraldas Ecuador, using ion exchange resins. *Journal of Natural Sciences Research.* **2017**, 80-92.
- [29] Soledispa B. and Villacreses J. Estudio Composicional de las arenas ferrotitaníferas del sector comprendido entre el Estero Data de Posorja y el Monasterio de Santa Teresa, Provincia de Guayas Ecuador. INOCAR, *Acta Oceanografica del Pacifico.* **1990**.

- [30] Trujillo D. and Managon L. Titanium dioxide recovery from ilmenite contained in ferrotitaniferous sands from Mompiche Ecuador. *Journal of Geological Resource and Engineering*. **2016**, 175-183.
- [31] Valderrama L., Poblete R., Contreras C., 2005. Caracterizacion y Concentracion de Muestras de Arenas de Caldera, Region Atacama. *Revista de la Facultad de Ingenieria, Universidad de Atacama*, **2005**, 19, 38-44.
- [32] Toro, J., Ayala, C., Chimarro, M., Vera, D., Caetano, M. Ricaute, M. Oceanic processes controlling grain-size and granulometric parameters of beach sands in coastal Ecuador. Yachay Tech University, November 14, **2019**.
- [33] Nordeste, U. N. del. Trabajo Práctico N°4: Volumetria de Precipitación. **2010**, 3, 3.
- [34] Rigas, F.; Morales, A. A.; Navarrete, M. Assessment of Copper Slag as a Sustainable Fenton-Type Photocatalyst for Water Disinfection. **2014**, 199–227.
- [35] Chakraborty, S.; Chowdhury, S.; Das Saha, P. Adsorption of Crystal Violet from Aqueous Solution onto NaOH-Modified Rice Husk. *Carbohydr. Polym.* **2011**, 86 (4), 1533–1541.
- [36] Cho, B. P.; Yang, T.; Blankenship, L. R.; Moody, J. D.; Churchwell, M.; Beland, F. A.; Culp, S. J. Synthesis and Characterization of N-Demethylated Metabolites of Malachite Green and Leucomalachite Green. *Chem. Res. Toxicol.* **2003**, 16 (3), 285–294.
- [37] Ahmad, R. Studies on Adsorption of Crystal Violet Dye from Aqueous Solution onto Coniferous Pinus Bark Powder (CPBP). *J. Hazard. Mater.* **2009**, 171 (1–3), 767–773.
- [38] Liu, W.; Chao, Y.; Yang, X.; Bao, H.; Qian, S. Biodecolorization of Azo, Anthraquinonic and Triphenylmethane Dyes by White-Rot Fungi and a Laccase-Secreting Engineered Strain. *J. Ind. Microbiol. Biotechnol.* **2004**, 31 (3), 127–132.
- [39] Schnick RA The impetus to register new therapeutants for aquaculture. *Prog Fish.* **1988**.
- [40] Velmurugan Dhinakaran. Dye removal from aqueous solution using low cost adsorbent. *International Journal of Environmental Sciences* **2011** , 1, 1492-1503.

- [41] Maria, P. u. Novel materials based on fly ash for advanced industrial wastewaters treatment. *Msc. thesis, Malaysia: University of Sains*. **2014**.
- [42] Durairaj, S. D., Shankar. Colour removal from textile industry wastewater using low cost adsorbents. *International Journal of Chemical, Environmental and Pharmaceutical Research*, **2012**, 3, 52-57.
- [43] Beyene, H. D. The potential of dyes removal from textile wastewater by using different treatment technology. *International Journal of Environmental Monitoring and Analysis***2014**, 2, 347-353,
- [44] Ramakrishna, M. Biomimetic synthesis of hybrid materials for potential applications. Singapore: *Msc. thesis, National University of Singapore*. **2013**
- [45] Gautam, R. K.; Chattopadhyaya, M. C. Remediation Technologies for Water Cleanup: New Trends. *Nanomater. Wastewater Remediat.* **2016**, 19–32.
- [46] Andreozzi, R.; Caprio, V.; Insola, A.; Marotta, R. Advanced Oxidation Processes (AOP) for Water Purification and Recovery. *Catal. Today* **1999**, 53 (1), 51–59.
- [47] IQD Invesquia, S. . Procesos de Oxidación Avanzada. *IQD Invesquia, S.L* **2010**, 4.
- [48] I. Litter, M.; Quici, N. Photochemical Advanced Oxidation Processes for Water and Wastewater Treatment. *Recent Patents Eng.* **2011**, 4 (3), 217–241.
- [49] Fernández-alba, A. R. Vt.
- [50] Castañeda, A. Procesos de Oxidación Avanzada Aplicados En El Tratamiento de Aguas de La Industria Del Petróleo. *Especialización En Recursos Hidráulicos y Medio Ambiente*. **2014**.
- [51] Pavas, E.; Olaya, L.; Uribe, M.; Agudelo, D. Degradación de Colorantes de Aguas Residuales Empleando $UV/TiO_2/H_2O_2/Fe$. *Rev. Univ. EAFIT* **2012**, 43 (146), 80–101.
- [52] Kiki J, Pulgarin C, Peringer P, Gratzel M. Beneficial effects of homogeneous photo-Fenton pretreatment upon the biodegradation of anthraquinone sulfonate in waste water treatment. *Appl. Catal. B: Environ.* **1993** 3(1):85-99.

- [53] Faust B, Hoigne J. Photolysis of Fe(III)-hydroxy complexes as sources of OH radicals in clouds, fog and rain. *Atmos. Environ.* **1990** 24A:79-89.
- [54] Un, U.; Mixto, Ó. DE DESECHOS POR EL PROCESO FOTO-FENTON HETEROGÉNEO. **2016**, 28, 574-582.
- [55] Reddy PVL, Kim KH. A review of photochemical approaches for the treatment of a wide range of pesticides. *Journal of Hazardous Materials.* **2015**, 285:325-335.
- [56] Coronado JM, Fresno F, Hernández-Alonso MD, Portela R. Design of advanced photocatalytic materials for energy and environmental applications. *In: Green Energy and Technology.* 1st ed. London: Springer-Verlag; **2013**. 351 p.
- [57] GAYA UI. Heterogeneous Photocatalysis Using Inorganic Semiconductor Solids. 1st ed. *Dordrecht: Springer Science + Business Media;* **2014**. 222 p.
- [58] Zhao C, Pelaez M, Dionysiou DD, Pillai SC, Byrne JA, O'shea KE. UV and visible light activated TiO₂ photocatalysis of 6-hydroxymethyluracil, a model compound for the potent cyanotoxin cylindrospermopsin. *Catalysis Today.* **2014**;224:70-76.
- [59] Spasiano D, Marotta R, Malato S, Fernandez-Ibañez P, Somma I. Solar photocatalysis: Materials, reactors, some commercial, and pre-industrialized applications. A comprehensive approach. *Applied Catalysis B: Environmental.* **2015**;170-171:90-123.
- [60] Wang W, Huang G, Yu JC, Wong PK. Advances in photocatalytic disinfection of bacteria: Development of photocatalysts and mechanisms. *Journal of Environmental Science.* **2015**;34: 232-247.
- [61] Marschall R, Wang L. Non-metal doping of transition metal oxides for visible-light photocatalysis. *Catalysis Today.* **2014**;225:111-135.
- [62] M. A. Mohamed, W. N. Wan Salleh, J. Jaafar, M. S. Rosmi, Z. A. Mohd. Hir, M. Abd Mutalib, A. F. Ismail and M. Tanemura, *Appl. Surf. Sci.* **2017**, 393, 46.
- [63] Loaiza, D. Obtención de Dióxido de Titanio (TiO₂), a partir de Ilmenita (FeTiO₃), presente en arenas ferrotitaníferas provenientes del sector Congüime, cantón Paquisha, provin-

- cia de Zamora Chinchipe. *Tesis de Pregrado*, Universidad Técnica Particular de Loja, Loja. **2017**.
- [64] Soledispa, B.; Villacres, J. Estudio Composicional de Las Arenas Ferrotitaníferas Del Sector Compreendido Entre El Estero Data de Posorja y El Monasterio de Santa Teresa, *Provincia Del Guayas, Ecuador*. **1990**.
- [65] Trujillo, D. Desarrollo de Un Proceso de Recuperación de Dioxido de Titanio a Partir de Ilmenita Presente En Las Arenas Ferrotitaníferas de La Zona de Mopinche. **2015**, 193.
- [66] D. Kanakaraju, et al., Titanium dioxide/zeolite integrated photocatalytic adsorbents for the degradation of amoxicillin, *Appl. Catal. B: Environ* **2015**. 166–167 45–55.
- [67] S. Gomez, et al., In situ generated TiO₂ over zeolitic supports as reusable photocatalysts for the degradation of dichlorvos, *Appl. Catal. B: Environ* **2015** . 162, 167–173.
- [68] O.E. Jaime-Acuña, et al., Disperse orange 30 dye degradation by assisted plasmonic photocatalysis using Ag-CdZnSO/zeolitic matrix nanocomposites, *Catal. Commun* **2016**. 75, 103–107.
- [69] F. Haque, et al., Preparation and performance of integrated photocatalyst adsorbent (IPCA) employed to degrade model organic compounds in synthetic wastewater, *J. Photochem. Photobiol. A Chem.* **2005** 169 (1) 21–27.
- [70] N.F. Zainudin, A.Z. Abdullah, A.R. Mohamed, Characteristics of supported nano TiO₂/ZSM-5/silica gel (SNTZS): photocatalytic degradation of phenol, *J. Hazard. Mater.* **2010** 174 (1–3) 299–306.
- [71] M. Khatamian, S. Hashemian, S. Sabaee, Preparation and photo-catalytic activity of nano-TiO₂-ZSM-5 composite, *Mater. Sci. Semicond. Process* **2010**. 13 (3) 156–161.
- [72] A.N. Ökte, Ö. Yılmaz, Characteristics of lanthanum loaded TiO₂-ZSM-5 photocatalysts: decolorization and degradation processes of methyl orange, *Appl. Catal* **2009**. A 354 (1–2) 132–142.
- [73] A. Neren Ökte, Ö. Yılmaz, Photodecolorization of methyl orange by yttrium incorporated TiO₂ supported ZSM-5, *Appl. Catal. B: Environ.* **2008**. 85 (1–2), 92–102.

- [74] C. Zhao, et al., Advantages of TiO₂/5A composite catalyst for photocatalytic degradation of antibiotic oxytetracycline in aqueous solution: comparison between TiO₂ and TiO₂/5A composite system, *Chem. Eng. J* **2014**, 248, 280–289.
- [75] Y. Chen, K. Liu, Preparation and characterization of nitrogen-doped TiO₂/diatomite integrated photocatalytic pellet for the adsorption-degradation of tetracycline hydrochloride using visible light, *Chem. Eng. J* **2016**, 302, 682–696.
- [76] Q. Zhang, et al., TiO₂ nanotube-carbon macroscopic monoliths with multimodal porosity as efficient recyclable photocatalytic adsorbents for water purification, *Mater. Chem. Phys* **2016**, 173, 452–459.
- [77] M. Akkari, et al., ZnO/clay nanoarchitectures: synthesis, characterization and evaluation as photocatalysts, *Appl. Clay Sci* **2016**, 131, 131–139.
- [78] S. Vadivel, et al., Graphene oxide–BiOBr composite material as highly efficient photocatalyst for degradation of methylene blue and rhodamine-B dyes, *J. Water Process Eng* **2014**, 1, 17–26.
- [79] V. Vimonses, et al., An adsorption–photocatalysis hybrid process using multifunctional-nanoporous materials for wastewater reclamation, *Water Res* **2010**, 44 (18) 5385–5397.
- [80] S. Bera, et al., Hierarchically structured ZnO-graphene hollow microspheres towards effective reusable adsorbent for organic pollutant via photodegradation process, *J. Alloys Compd* **2016**, 669, 177–186.
- [81] C. Fan, et al., Fabrication of 3D CeVO₄/graphene aerogels with efficient visible- light photocatalytic activity, *Ceram. Int* **2016**, . 44 (18), 10487–10492.
- [82] S. Basha, et al., Studies on the adsorption and kinetics of photodegradation of pharmaceutical compound, indomethacin using novel photocatalytic adsorbents (IPCAs), *Ind. Eng. Chem. Res* **2010** 11302–11309.
- [83] J.G. McEvoy, Z. Zhang, Synthesis and characterization of Ag/AgBr-activated carbon composites for visible light induced photocatalytic detoxification and disinfection, *J. Photochem. Photobiol. A Chem.* **2016**, 321, 161–170.

- [84] F.-P. Chen, et al., Electrochemical preparation of uniform CuO/Cu₂O heterojunction on beta-cyclodextrin-modified carbon fibers, *J. Appl. Electrochem.* **2016** 379–388.
- [85] T. Kamal, et al., Adsorption and photocatalyst assisted dye removal and bactericidal performance of ZnO/chitosan coating layer, *Int. J. Biol. Macromol* **2015**, 81, 584–590.
- [86] S. Wang, S. Zhou, Photodegradation of methyl orange by photocatalyst of CNTs/P-TiO₂ under UV and visible-light irradiation, *J. Hazard. Mater* **2011**, 185, 77–85.
- [87] M. Ahmad, et al., Graphene–Ag/ZnO nanocomposites as high performance photocatalysts under visible light irradiation, *J. Alloys Compd.* **2013**, 577, 717–727.
- [88] T. Nakajima, et al., Combined use of photocatalyst and adsorbent for the removal of inorganic arsenic(III) and organoarsenic compounds from aqueous media, *J. Hazard. Mater* **2005**. 120 (1–3), 75–80.
- [89] A. Nasrollahpour, S.E. Moradi, Photochemical degradation of methylene blue by metal oxide-supported activated carbon photocatalyst, *Desal. Water Treat.* **2016** 8854–8862.
- [90] M. Zhang, et al., Separation free C₃N₄/SiO₂ hybrid hydrogels as high active photocatalysts for TOC removal, *Appl. Catal. B: Environ.* **2016**, 194, 105–110.
- [91] W. Qiu, et al., Efficient removal of Cr(VI) by magnetically separable CoFe₂O₄/ activated carbon composite, *J. Alloys Compd* **2016**, 678, 179–184.
- [92] S. Sohrabnezhad, A. Pourahmad, M. Razavi, Silver bromide in montmorillonite as visible light-driven photocatalyst and the role of montmorillonite, *Appl. Phys. A: Mater. Sci. Proces.* **2016**, 122 (9)
- [93] Serin, F. G., Selen. Adsorption study on orange peel: Removal of Ni(II) ions from aqueous solution. *African Journal of Biotechnology* , **2012**. 11, 1250-1258.
- [94] Asgher, M. Utilization of citrus waste biomass for sorption of reactive dyes from aqueous solutions. *International Journal of Environmental Science.* **2012**, 3, 179-191.
- [95] Nader Yousefi, A. F. Adsorption of Reactive Black 5 dye onto modified wheat straw, isotherm and kinetics study. *Sacha Journal of Environmental studies.* **2011** , 1, 81-91.

- [96] Langmuir, I.: The constitution and fundamental properties of solids and liquids. *Journal American Chemical Society* **1916**. 2221-2295.
- [97] Doğan, M., Alkan, M., Onganer, Y. Adsorption of methylene blue from aqueous solution onto perlite. *Water Air and Soil Pollution* **2000**.120, 229-249.
- [98] Kinniburgh, D.G. General purpose adsorption isotherms. *Environmental Science and Technology*. **1986** 895-904.
- [99] Longhinotti, E., Pozza, F., Furlan, L., Sanchez, M.D.N.D., Klug, M., Laranjeira, M.C.M., Favere, V.T. Adsorption of anionic dyes on the biopolymer chitin. *Journal Brazilian Chemical Society*. **1998**. 435-440.
- [100] Freundlich, H.M.F. Über die adsorption in lösungen. *Zeitschrift für Physikalische Chemie (Leipzig)*. **1906**. 385-470.
- [101] Halsey, G.D. The role of surface heterogeneity. *Advanced Catalysis* **1952**. 4: 259-269.
- [102] Temkin, M.J., Pyzhev, V. Acta Physiochim, *URSS* **1940**.12, 217-222.
- [103] Kavitha, D., Namasivayam, C. Experimental and kinetic studies on methylene blue adsorption by coir pith carbon. *Bioresource Technology*. **2007** 14-21.
- [104] Aharoni, C., Ungarish, M. Kinetics of activated chemisorption. Part 2. Theoretical models. *Journal Chemical Society, Faraday Trans.* **1977** 456-464.
- [105] Aharoni, C., Sparks, D.L. Kinetics of Soil Chemical Reactions – A Theoretical Treatment, in Sparks DL and Suarez DL (Eds). *Rate of Soil Chemical Processes, Soil Science Society of America*, Madison, WI. **1991**. 1-18.
- [106] Pearce, C.I., Lloyd, J.R., Guthrie, J.T. The removal of color from textile wastewater using whole bacterial cells: a review. *Dyes Pigments*. **2003**. 179-196.
- [107] Akkaya, G., Ozer, A. Adsorption of acid red 274 (AR 274) on *Dicranella varia*: determination of equilibrium and kinetic model parameters. *Process Biochemistry*. **2005**. 3559-3568.
- [108] Radushkevich, L.V. Potential theory of sorption and structure of carbons. *Zhurnal Fizicheskoi Khimii*. **1949** 1410-1420.

- [109] Dubinin, M.M. The potential theory of adsorption of gases and vapors for adsorbents with energetically non-uniform surface. *Chemical Review*. **1960**. 235-266.
- [110] Kundu, S., Gupta, A.K. Investigation on the adsorption efficiency of iron oxide coated cement (IOCC) towards As (V)-Kinetics, equilibrium and thermodynamic studies. *Colloids Surface A: Physicochemical Engineering Aspects*. **2006** 121- 128.
- [111] Husein, M. a. Removal of strontium from aqueous solutions by adsorption Onto orange peel: isotherms, kinetics, and thermodynamic studies. *Journal of Chemical Engineering*. **2012** 3, 181-189.
- [112] Muhi Mohammed, F. Modelling and design of water treatment processes using adsorption and electrochemical regeneration. *Msc.thesis, University of Manchester*. **2011**.
- [113] Koyuncu, M. Removal of Maxilon Red GRL from aqueous solutions by adsorption onto silica. *Oriental Journal of Chemistry*. **2009**. 25, 35-40.
- [114] Lagergren, S. Zur theorie der sogenannten adsorption geloster stoffe. *Kungliga Svenska Vetenskapsakademiens. Handlingar*. **1898** 1-39.
- [115] Ho, Y.S., Chiu, W.T., Wang, C.C. Regression Ahmed El Nemr et al. analysis for the sorption isotherms of basic dyes on sugarcane dust. *Bioresource Technology*. **2005** 1285–1291.
- [116] Zeldowitsch, J. Über den mechanismus der katalytischen oxidation von CO and MnO₂. *Acta Physicochim. URSS* 1:**1934**. 364-449.
- [117] Chien, S.H., Clayton, W.R. Application of Elovich equation to the kinetics of phosphate release and sorption on soils. *Soil Science Society American Journal* . **1980**. 265-268.
- [118] Sparks, D.L. Kinetics of reaction in Pure and Mixed Systems, in Soil Physical Chemistry. *CRC Press, Boca Raton*. **1986**.
- [119] Weber, W.J., Morris, J.C. Kinetics of adsorption on carbon from solution. Journal Sanit. Engineering Division. *American Society Civil Engineering*. **1963**. 31-60.
- [120] Srinivasan, K., Balasubramanian, N., Ramakrishan, T.V. Studies on chromium removal by rice husk carbon. *Indian Journal of Environtal Health*. **1988**. 376-387.

Appendices

A Appendix 1.

A.1 Crystal Violet Dye

Crystal violet (CV) or gentian violet also known as methyl violet 10B or hexamethylpararosani-line chloride, a cationic triphenylmethane dye derived from aniline (Figure 21), and to commercial mixture of triphenylmethane dyes with hexamethylpararosani-line chloride as the pre-dominant constituent (Table 21) [10].

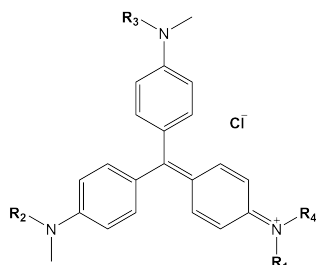


Figure 21: Structure of Crystal Violet

Table 21: Composition of commercial Crystal Violet

Typical Composition of Commercial Gentian Violet	Substituent				% Concentration
	R_1	R_2	R_3	R_4	
Hexamethylpararosani-line chloride [Gentian Violet; Crystal Violet]	CH ₃	CH ₃	CH ₃	CH ₃	Typically >96%
Pentamethylpararosani-line chloride [Methyl Violet]	CH ₃	CH ₃	CH ₃	H	
N,N,N',N'-Tetramethylpararosani-line chloride	H	CH ₃	CH ₃	H	
N,N,N',N'-Tetramethylpararosani-line chloride	CH ₃	CH ₃	H	H	If present, typically <4%
N,N',N'-Trimethylpararosani-line chloride	CH ₃	H	H	H	
N,N',N'-Trimethylpararosani-line chloride	CH ₃	H	H	H	If present, typically trace

Crystal Violet (CV) dye has been used in human and veterinary medicine and also as a dye in textile and paper industries [9]. The medical community also applies CV as a biological stain. The dye is also used as an external skin disinfectant in humans and animals [35].

The CV is reported as a recalcitrant molecule that persists in the environment for a long time and has toxic effects on aquatic as well as terrestrial life [9]. In vitro investigations have revealed that CV acts as a mitotic poison, potent carcinogen and promotes tumor growth in some species of fish[36]. Hence, CV is regarded as a biohazard substance. The dye is also found to cause moderate eye irritation, painful sensitization to light and permanent injury to the cornea since the product is a cationic dye, which is highly toxic to mammalian cells. Nevertheless, in extreme cases, it may lead to respiratory and kidney failures [37].

The dark-colored wastewater containing CV significantly affect the photosynthetic activity of aquatic plants because of reduced sunlight penetration and may also be toxic to some other aquatic life due to the presence of aromatics, metals, and chlorides etc.[38] Due to its adverse effects on human health, CV has been listed as hazardous chemical or material and its use has been prohibited in aquaculture and food industry. However, it is still used in some areas due to its relatively low cost, ready availability, and efficacy[39]. Hence, the removal of CV from wastewater of different industries is essential to not only protect human health but also for the protection of soil and water ecosystems.

A.2 Techniques of wastewater treatment

Pollution by organic chemicals including dyes is one of the most serious environmental problems facing life on earth. These dyes have a variety of complex organic compounds and toxic substances with unknown environmental behavior such as aromatic amines ($C_6H_5 - NH_2$), which are suspected to have carcinogenic effects. The resistance of these organic compounds to decomposition due to their complex chemical structure results in difficult to treat [40]. Many researchers have studied different methods to remove dyes from wastewater including chemical and physicochemical processes such as, adsorption, chemical precipitation, electrochemical oxidation, and chemical oxidation processes [41]. Several reported methods for the removal of dye pollutants from wastewater are summarized in Appendix C.

Different physical methods are widely used, such as membrane-filtration processes and ad-

sorption techniques. Liquid-phase adsorption is one of the most popular methods for the removal of pollutants from wastewater since it produces a high-quality treated effluent. This process is an attractive alternative for the treatment of contaminated waters, especially if the adsorbents are inexpensive and do not require an additional pretreatment step before its application [43]. The major disadvantages of these kinds of processes are a limited lifetime before membrane fouling occurs and the cost of periodic replacement [42].

Chemical methods include coagulation or flocculation, precipitation, electrokinetic coagulation, advanced oxidation processes, or electrochemical process. Although these methods are efficient for the treatment of wastewater contaminated, they are very costly, commercially unattractive, require high electrical energy demand, the consumption of chemical reagents and accumulation of concentrate sludge creates disposal problems [41, 43]

A.3 Adsorption

Adsorption technology is a physical technique, which is a promising treatment option for pollutant removal due to its efficiency, simplicity, inexpensive and it is not toxic [11, 12]. In the process of adsorption, the substance gets separated from the liquid phase and gets accumulated on the adsorbent [13]. When solely utilized, this method is unable to eliminate or destroy the pollutants completely, but rather concentrates the pollutants through adsorption and separates it from the system. Various adsorbents have been reported in published works for the removal of pollutants such as activated carbon, clays, zeolite, and polymeric adsorbents [14, 15, 16, 17].

Zeolites are aluminosilicates minerals that contain aluminum, silicon, and oxygen in their structure. Zeolite is one of the most important adsorbents due to its high extensive surface area, a charged framework with amphoteric properties and high adsorption capacity [18]. Besides, its unique Al-O bonds in zeolite structure that able to reduce the electron electron-hole recombination process, making it a promising candidate for hybrid adsorbents-photocatalyst applications [19].

A.4 Advanced Oxidation Processes (AOPs)

Advanced oxidation processes (AOPs), consist of generations of chemical oxidants such as hydroxyl radicals, which is an important class of technology for accelerating the oxidation and

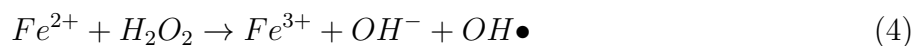
destruction of a wide range of organic contaminants from wastewater [?]. The $OH\bullet$ radicals are powerful, non-selective, and highly effective oxidants and react effectively with most of the organic compounds [45, 46]. Besides the generation of radicals is made from oxygen, hydrogen peroxide (H_2O_2), UV radiation, iron salts [Fe(II) y Fe(III)] and catalysts such as titanium dioxide (TiO_2) [46, 48, 49, 50], so the reaction by-products are only water and carbon dioxide [47]. The AOPs can be classified as non-photochemical processes and photochemical processes based on the participation of light in the process (Table 22) [50, 51].

Table 22: Classification of AOPs

Non-photochemical processes	Photochemical processes	Solar photocatalysis
<ul style="list-style-type: none"> • Ozonization • Ozonization with H_2O_2/O_3 • Fenton processes and related • Electrochemical oxidation • Radiolysis and treatment with electron beams • Non-thermal plasma • Oxidation in a sub and super-critical cater 	<ul style="list-style-type: none"> • Vacuum ultraviolet • UV/H_2O_2 • UV/O_3 • $UV/H_2O_2/O_3$ 	<ul style="list-style-type: none"> • Homogeneous photocatalysis (Photo-Fenton) • Heterogeneous Photo-Fenton • Heterogeneous photocatalysis Photocatalysis mechanism with TiO_2

A.4.1 Photo-Fenton and Heterogeneous Photo-Fenton

In Fenton processes, the generation of the hydroxyl radicals takes place from the decomposition of hydrogen peroxide catalyzed by an iron salt, as shown in eq (4):



The kinetics of the Fenton reaction can be increased by the irradiation of visible light and UV light [52]. The photo-Fenton process becomes catalytic when Fe^{3+} is reduced back to Fe^{2+} by radiation, as shown in eq (5):



Due to this, oxidation of the ferrous ion continues to occur due to the oxidative action of hydrogen peroxide, while thanks to the photo-reduction, the accumulated ferric ion is reduced to ferrous ion. Thus, the regenerated ferrous ion reacts again with hydrogen peroxide generating hydroxyl radicals in a continuous cycle [53]. Considering that one of the main disadvantages of the homogeneous Fenton process is the need for a neutralization stage to separate iron, researchers are currently focused on the development of solid catalysts that incorporate iron into their structure for the decomposition of hydrogen peroxide, such as Ilmenite, Hematite, Magnetite, etc. This process is known as heterogeneous Fenton [54].

A.4.2 Heterogeneous Photocatalysis with TiO_2

Heterogeneous photocatalysis is an interesting alternative process that can remove the contaminants at ambient temperature and pressure by oxidation. Titanium dioxide is used as a photocatalyst due to its bandgap that is 3.2 eV, and also because (TiO_2) is non-toxic, chemically stable, commercially available, inexpensive, and environmentally friendly. In this process, very reactive oxygen species are generated from the catalyst titanium dioxide induced by ultraviolet or visible radiation [55]. The titanium dioxide capacity to absorb energy and degrade molecules is due to the energy bands created by atomic orbitals arranged when a new compound is formed on the surfaces of the titanium dioxide. These regions are denominated conduction band (CB) and valence band (VB)[56]. In titanium dioxide, there will be a region without available energy levels, which are described as bandgap [57]. Figure 22. The electron (e) in the CB can interact with oxygen molecules and form reactive groups, such as the hydroxyl ($OH\bullet$) and superoxide ($O\bullet$) radicals and single oxygen (1O_2) [58, 59, 60]. On the other hand, the vacancies (h^+) created due to the electrons transfer are oxidants with the potential to convert water molecules in $OH\bullet$ [61].

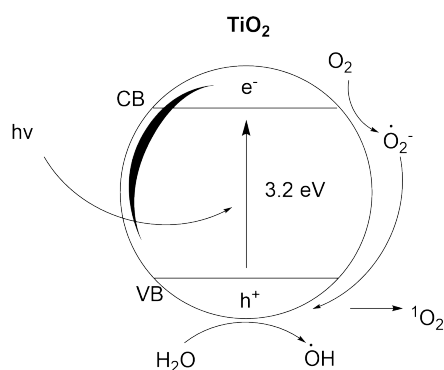


Figure 22: Semiconductors photocatalytic mechanism..

A.5 Integrated Photocatalyst Adsorbents (IPCA)

The integration of adsorption and photocatalysis process gives several benefits to wastewater treatment. This hybrid process would be able to remedy the disadvantages of each technique when operated individually and hence improve the removal efficiency. A lot of studies have been reported in employing IPCA for contaminant degradation in wastewater, these studies are listed in the appendix ???. Most of these studies reported on the improvement of degradation efficiency due to the increment in contaminant adsorption on the photocatalyst surface by the adsorbents. It is surprising that the numbers of publications concerning IPCA are very limited, approximately only 13.7% from total publications about photocatalyst for wastewater treatment from 1989 to 2018 [20].

One of the materials recently studied by the scientific community and that has shown adsorbent and photocatalytic nature is the Hematite due to its crystalline structure and its narrow Band-Gap of 2.2 and makes it an ideal mineral for the integrated photocatalysis and adsorption process [23].

Previous studies have been proposed a reaction mechanism between IPCA and target compound. Figure 23 shows the proposed of a general photocatalytic degradation reaction mechanism. First, Dye adsorption occurs mainly through surface complexation as well as coagulation on the surface of IPCA. Then, during the process of the semiconductor-initiated photocatalytic reaction, IPCA can create electron-hole e^-/h^+ pairs upon UV-Visible light excitation. The photogenerated electrons on the surface of IPCA may react with O_2 and H_2O to generate $O_2^{\bullet-}$ and OH^{\bullet} radical and other reactive oxygen species. [62].

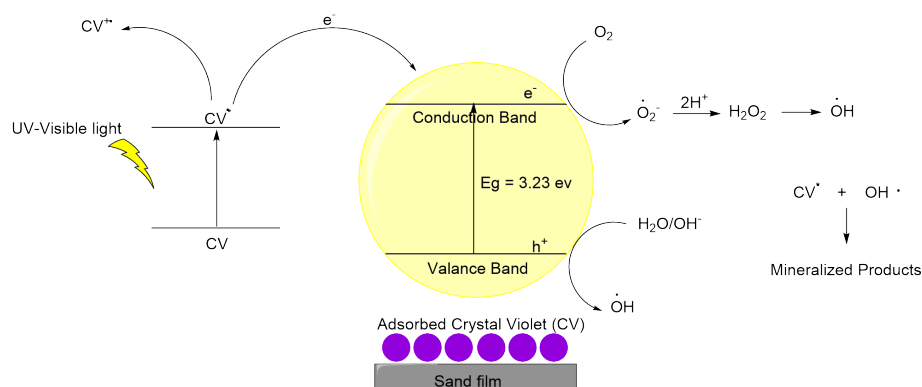


Figure 23: Schematic integrated adsorption and degradation of CV over Sands under UV-visible-light illumination.

A.6 Black Sands

Black Sands, also known as ferrotitaniferous sands, they are a natural combination of heavy minerals that are mostly made of iron oxides and titanium oxides, with traces of metals such as manganese (Mg), magnesium (Mg), aluminum (Al), calcium (Ca), vanadium (V) and chromium (Cr). The Black sands are constituted by minerals such as Magnetite (Fe_3O_4), Ilmenite ($FeO \cdot TiO_2$), Hematite (Fe_2O_3), rutile (TiO_2), Zircon ($ZrSiO_4$) and different silicates like Quarts (SiO_2) [63].

A.6.1 Deposits of Black sands in Ecuador

Several studies carried out in Ecuador show that the beaches located in the coastal strip, mainly in the provinces of Guayas, Manabí and Esmeraldas, have potential deposits of ferrotitaniferous black sands, whose mineralogical resources (mainly Fe and Ti) have not been fully exploited[64]. Currently, Scientific community are proposing projects that take advantage of Ecuador's non-renewable natural resources, such as black sands, thus contributing to the change in the productive matrix of Ecuador [65].

B Appendix 2.

Table 23: Table of Classification of Dyes in Textile Industry

Classification of Dyes		
Dye type	Characteristics	Examples
According to Chemical Structure		
Nitro Dyes	Polynitro derivatives of phenols containing at least one nitro group ortho or para to the hydroxyl group.	Picric acid, Maritus yellow and Naphthol yellow S
Azo dyes	The azo dyes represent the largest and the most important group of dyes. They are characterized by the presence of one or more azo groups ($-N=N-$), which form bridges between two or more aromatic rings.	Aniline yellow, Butter yellow, Chrysoidine, Methyl Orange, Orange II, Para Red, Resorcin Yellow, Disperse Red 1, Congo Red.
Diphenylmethane dyes	-	Auramine O
Triphenylmethane dyes	Central carbon atom is joined to two benzene rings and to p-quinoid group. Triphenylmethane dyes are not fast to light or washing, however, except when applied to acrylic fibers. They are used in large quantities for coloring paper, and typewriter ribbons where fastness to light is not so important.	Malachite Green, Pararosaniline, Rosaniline, Crystal Violet
Xanthene dyes	Obtained by condensing phenols with phthalic anhydride in the presence of zinc chloride, sulphuric acid, or anhydrous oxalic acid.	Fluorescein, eosin, and Rhodamine B.
Phthaeleins	Phthaeleins are related to xanthene dyes	Phenolphthalein.

Indigoid and Thioindigoid dyes	Indigoid is the parent compound of indigoid dyes.	Tyrian Purple, Thioindigo.
Anthraquinoid dyes	A p-quinoid group is fused to two other benzene rings.	Alizarin
According to Method of Application		
Direct dyes	These contain acidic or basic groups and combine with polar groups in the fiber. Such dyes color a fabric directly when the fiber is immersed in a hot aqueous solution of the dye.	Naphthol Yellow S and Martius Yellow
Mordant dyes	This class of dyes requires a pre-treatment of the fiber with a mordant material designed to bind the dye. The mordant becomes attached to the fiber and then combines with the dye to form an insoluble colored complex. Commonly used mordant are the oxides of aluminum, iron and chromium.	Alizarin
Vat dyes	These dyes are insoluble in water, but on reacting with sodium hydrosulphite yield alkali soluble forms (Leuco-compounds) which may be colorless. It is in this form they are introduced into the fabric. After the reduced dye has been absorbed in the fiber, the original insoluble colored dye is reformed by oxidation with air or chemicals.	Indigo
Ingrain dyes	These dyes are synthesized within the fabric, and may be applied to any type of fiber.	Azo dyes

Disperse dyes	These are insoluble in water, but are capable of dissolving certain synthetic fibers. The absorption into the fiber is carried out at high temperatures and pressures.	Celliton Fast Pink B and Celliton Fast Blue B
---------------	--	---

C Appendix 3.

Table 24: Photochemical and Non-photochemical processes

Non-Photochemical processes	
Non-Photochemical Process	Description
Ozonation in aqueous medium (O_3/OH^-)	The Ozono can react in direct form with a organic substrate through a slow and selective reaction or through a radical reaction favored in alkaline medium, fast and non-selective.
Ozonation with hydrogen peroxide (O_3/H_2O_2)	Ozonation transforms the contaminates en simple compounds, more refractive than the reactive. An improvement is achieved by adding hydrogen peroxide (H_2O_2) that is a weak acid, a strong oxidant and a unstable compound.
Fenton Process Fe^{2+}/H_2O_2	The combination of Fe^{2+} with H_2O_2 generates radicals $OH\bullet$, which in turn will react in two ways: Oxidation on Fe(II) and the attack of the organic matter.
Electrochemical oxidation	The application of a electric current(2-20A) between two electrodes in water produce primary chemical reactions that will generate radicals, these radicals will oxidize organic matter.
Radiology and electron beam treatment	These processes are based on the generation on highly reactive electrons, radical ions and neutral radicals by exposure of the waters to be treated to massive particle beams or high energy electromagnetic waves. It can use γ rays, x rays and electron beam accelerators such as the Van-de-Graaf type or the linear ones. When the beam of electrons penetrate the water, electrons lose energy for non-elastic collisions with molecules of H_2O y reactive species are generates.

Non-thermal plasma	Plasma is considered as a four state of matter that contains ions and free electrons (electric gas). Plasma can be generated, non-thermally, by an electric shock or bombardment of a gas with a high-energy electron beam; The energy of the electrons in the plasma is 10 eV, equivalent to high temperatures. These plasmas are good sources of highly reducing and oxidizing reactive species, such as: O (3P), OH, N, H, NH, CH, O ₃ .
Electrohydraulic discharge - Ultrasonic	This technology uses high power ultrasound (from 15kHz until 1MHz), and takes advantage of electrohydraulic cavitation, that is, the growth and cyclic collapse of gas bubbles. The gas explodes and very very high local temperatures and pressures are reached (4000-10000K Y 1000-10000 bares in the center of the collapsed bubbles). Degradation of organic matter take place through the reactions with radicals generated by thermal reaction, or by reactions in presence of oxygen.
Sub and Super-critical oxidation in water	The process that operates in critical conditions is also called oxidation in moist air. This process work at pressures between 10-220 bars and temperatures between 150-350°C. The mechanism involves the primary carbonation of the organic substrates and its subsequent reaction whit radicals OH that were produced en the catalytic transformation of O ₂ dissolved in the center carbon surface. The nitrogen, halogens and sulfur are mineralized too.
Photochemical processes	
Photochemical process	Description

Photolysis of water in the ultraviolet vacuum	It uses radiation with a wavelength less than UV-C (Less than 190 nm) that produce the degradation of organic matter in condensed or gaseous phases or the photolysis of water, which produces hydroxyl radicals, hydrogen atoms and aqueous electrons. $H_2O\bullet$. and $O_2^{\bullet-}$ are rapidly generated from the primary radicals.
UV/Hydrogen Peroxide	The photolysis of hydrogen peroxide is done using medium or low pressure mercury vapor lamps. In excess of hydrogen peroxide and with high concentrations of $OH\bullet$, competitive reactions take place that produce an inhibitory effect for degradation. The $OH\bullet$ are susceptible to recombine or react.
UV/ O_3	Combination of the UV/ H_2O_2 and O_3/H_2O_2 .
Photo-Fenton	Fenton's reaction increases its effectiveness by lighting irradiation due to several factors, including the additional reaction: $Fe(II)(OH)_2 + h\nu \rightarrow 2HO\bullet$
Ferrioxalate and other Fe(II) complexes	In the presence of organic ligands, such as carboxylic acids, Fe (III) can form stable complexes or associated ionic pairs that exhibit charge transfer bands from ligand to metal in the UV-Visible spectrum.
Heterogeneous Photocatalysis	It is based on the absorption of radiant energy (visible or uv) by a heterogeneous photocatalyst, which is normally a solid semiconductor. The reactions of destruction of the contaminants take place in the interfacial region between the catalyst and the solution.

D Appendix 4.

Table 25: Techniques of wastewater treatment

Advantages and disadvantages of the current methods of dye removal from industrial effluents		
Physical Chemical methods	Advantages	Disadvantages
Coagulation	Simple economically feasible.	High sludge production handling and disposal problems.
Floculation		
Electrokinetic coagulation		
Biodegradation	Economically attractive publicly acceptable treatment.	Slow process necessary to rate an optical favorable environmental, maintenance and nutrition requirements.
Adsorption on activate carbon	Good removal of wide variety of dyes. The most effective adsorbent, produce a high-quality treated effluent.	Very expensive. Ineffective against dispersing and vat dyes, the regeneration is expensive and results are loss of the adsorbent, non-destructive process.
Membrane separation	Remove all dye types, produces a high quality treated effluent.	Concentrated sludge production, high pressure, expensive, incapable of treating large volumes.
Ion exchange	Regeneration, no absorbent loss, rapid and effective process.	Economic contains, not effective for disperse dyes.
Selective bio adsorbents	Economically attractive, regeneration is not necessary, high selectivity.	Require chemical modification, non-destructive process.

Biomass	Low operating cost, good efficiency and selectivity, no toxic effects on microorganism.	A slow process, performance depends on some external factors (pH, salts).
Peat	Good adsorbent due to cellular structure.	Specific surface areas for adsorption areas lower than active carbon.
Wood chips	Good adsorption capacity for acid dyes.	Require a long retention times.
Silica gel	Effective for basic dyes removal.	Side reaction, prevent commercial applications.
Cucurbituril	Good. adsorption capacity for various dyes.	High cost.
NaOCl	Initiates and accelerates azo-bond cleavage.	Realize of aromatic amines.
Electrochemical destruction	Break clean compounds are non-hazardous.	High cost of electricity.
Oxidation	Rapid and efficient process.	High energy cost, chemical reagents.
Advanced oxidation process	No sludge production, little or no consumption of chemicals, efficiency for recalcitrant dyes.	Economically unfeasible formation by-products, technical constraints.
Fenton reagents	Effective discoloration of both soluble and insoluble dyes.	Sludge generation.
Ozonation	Applied a gaseous state, no alterations of volume.	Short half-life (20 min).
Photochemical	No sludge generation.	Formation of by-products.
Irradiation	Effective oxidation at lab scale.	Requires a lot of adsorbed O_2 .

E Appendix 5.

Table 26: Previous study on IPCA for organic contaminants degradation in waste water treatment

	Catalyst	Adsorbents	Target compound	Degradation efficiency	Ref.
1	TiO ₂	Zeolite	Amoxicillin	88 % (4 h irradiation time)	[66]
2	TiO ₂	Zeolite	Dichlorvos	89.96%	[67]
3	Ag-CdZnSO	Zeolite matrix	Disperse orange 30 dye	99.5% (90 min under UV light irradiation)	[68]
4	TiO ₂	Zeolite	Acetophenone, phenol, and chloroacetic acid	-	[69]
5	TiO ₂	Zeolite (ZSM-5)	Phenol	90% (180 min irradiation time)	[70]
6	Nano-TiO ₂	Zeolite (ZSM-5)	Brown-NG (an azo-dye)	100% (20 min under UV irradiation)	[71]
7	Lanthanum loaded-TiO ₂	Zeolite (ZSM-5)	Methyl orange	97% (210 min under UV irradiation)	[72]
8	Yttrium incorporated TiO ₂	Zeolite (ZSM-5)	Methyl orange	97.3%	[73]
9	TiO ₂	5 A Zeolite	Oxytetracycline (OTC)	30.57% (10 h under UV light irradiation)	[74]

10	N- doped TiO ₂	Diatomite	Tetracycline hydrochloride	90.2% (300 min irradiation time)	[75]
11	TiO ₂ nanotube	Carbon macroscopic monoliths	Methylene blue	100% (120 min)	[76]
12	ZnO	Clay	Methylene blue	100% (180 min)	[77]
13	BiOBr	Graphene oxide (GO)	Rhodamine-B (RhB) and methylene blue (MB)	98% (RhB, 45 min) and 95% (MB,30 min) under visible light	[78]
14	TiO ₂	Kaolin	Anions PO ₄ ³⁻ and NO ₃ ⁻	100% PO ₄ ³⁻ and 65% NO ₃ ⁻	[79]
15	ZnO	Graphene	Rhodamine B	100% (45 min irradiation time under UV light)	[80]
16	CeVO ₄	Graphene	Methylene blue	98% (18 min irradiation time under visible light)	[81]
17	TiO ₂	Activated carbon	Indomethacin	70%	[82]
18	Ag/AgBr	Activated carbon	Methyl orange (MO) and phenol	MO: 95.4% (2 h irradiation time under visible light) Phenol: 7.6 mg phenol per gram of composite in 3 h of irradiation	[83]

19	CuO/Cu ₂ O	-cyclodextrin modified carbon fibers	2, 6-dichlorophenol	87.5% (12 h irradiation time)	[84]
20	ZnO ₂	Chitosan	Methyl orange (MO)	80% (100 min irradiation time under UV light)	[85]
21	TiO ₂	CNT	Methyl orange (MO)	100% (100 min irradiation time under UV light)	[86]
22	Ag-ZnO	Graphene	Methylene blue (MB), rhodamine B and methyl orange (MO)	97.8% (7 h irradiation under sunlight)	[87]
23	TiO ₂	Activated alumina (AA)	Inorganic arsenic and organoarsenic compounds	98% (15 h under sunlight irradiation)	[88]
24	Fe ₃ O ₄	Modified activated carbon	Methylene blue	100% (75 min under UV light irradiation)	[89]
25	C ₃ N ₄	SiO ₂	Methylene blue	90% (4 h under visible light irradiation in dynamic systems)	[90]
26	CoFe ₂ O ₄	Activated carbon	Cr(VI)	Separation was efficient with magnetically separable Cr(VI)	[91]

27	Ag-CdZnSO	Zeolitic matrix	Disperse orange 30 dye	99.5% (90 min under UV light irradiation)	[68]
28	Ag-AgBr	MMT	Methylene blue	92% (20 min under visible light irradiation)	[92]

F Appendix 6.

UV-Vis diffuse reflectance spectroscopy.

There are several models to explain the intensity of diffuse reflected radiation, the most accepted is that of Kubelka and Munk, Fuller and Griffiths, where they demonstrate the following equation:

$$F(R) = (1 - R_d^2)/2R_d = \alpha/s \quad (6)$$

Where R_d is the relationship between the reflectance of the sample and that of a reference material (I/I_0), α is the absorption coefficient and s the dispersion coefficient. If the dispersion coefficient s is considered independent of the wavelength then the absorption coefficient is proportional to the Kubelka-Munk function.

$$F(R)s = \alpha \quad (7)$$

Substituting α in equation (6) for the optical determination of band energy, equation (8) is obtained where $h\nu$ is the photon energy in eV and E_g is the prohibited band energy.

$$\alpha(h\nu - E_b)^n/h\nu \quad (8)$$

$$[F(R)h\nu]^{1/n} = (h\nu - E_b) \quad (9)$$

In this way, calculations were made for the determination of band energy of the sand samples. For an energy absorption with a wavelength of 1022 nm the UV-Vis team reported an $F(R)$ value of 8.30 which was replaced in (9), for this equation it is known that the variable n takes a value of 0.5 in the case of a direct transition allowed and 2 for an indirect transition allowed. For an indirect transition of the black sand, the low band energy was determined considering the speed of light acceleration as $3 * 10^8 m/s$, radiation frequency ν of $2.94 * 10^{14}$ and Plank constant of $4.135 * 10^{-15}$ you have the value of $(h\nu F(R))^2$.

$$(h\nu F(R))^2 = ((4.135 * 10^{-15}) * (2.94 * 10^{14}) * (8.30))^2 \quad (10)$$

G Appendix 7

G.1 Adsorption isotherms

Adsorption is typically represented through isotherms, that is, the quantity of adsorbate on the adsorbent as a function of its pressure (in case of gas) or concentration (in case of liquid) at a constant temperature. Amount of adsorbate is almost continuously normalized by the mass of the adsorbent to permit comparison of various material. Equilibrium studies on adsorption process provide data on the capacity of the adsorbent [93].

The equilibrium state is characterized by a concentration of adsorbate (on the adsorbent as a function of it) in the solid phase ($q_e[mg/g]$) which is in dynamic equilibrium with a solute concentration in the liquid phase ($C_e[mg/L]$). A wide range values of q_e versus C_e values may be obtained by varying the amount of adsorbent (mg), the initial concentration of solute ($C_0[mg/L]$), and the volume of liquid [94]. The relationship between these q_e and C_e can normally be fitted to one or more equilibrium isotherm models. There are many models to describe the equilibrium behaviour for adsorption of contaminants from water [95].

Adsorption isotherms is a representation of the equilibrium adsorption capacity. $q_e[mg/g]$ measured at at different concentration plotted as a function of the equilibrium concentration ($C_e[mg/L]$) of solution studied.

The equilibrium experiment data can be analysed by different models like Langmuir, Freundlich, Temkin, Dubinin-Radushkevich, The Harkins-Hura model, etc.

G.1.0.1 Langmuir Model

The Langmuir model [96] assumes uniform energies of adsorption of a solute from a liquid solution onto a surface containing a definite number of identical sited as a mono-layer adsorption and no transmigration of adsorbate in the plane of the surface [97].

Therefore, the Langmuir isotherm model was chosen for estimation of the maximum adsorption capacity corresponding to complete monolayer coverage on the sorbent surface.

The Langmuir non-linear equation may be written as:

$$q_e = \frac{Q_m \cdot K_a \cdot C_e}{1 + K_L \cdot C_e} \quad (11)$$

Where, Q_m is a constant reflect a complete monolayer (mg/g), K_a is adsorption equilibrium constant (L/mg) that is related to the apparent energy of sorption [98, 99].

q_e = amount of dye adsorbed at equilibrium (mg/g)

C_e = equilibrium liquid-phase concentration (mg/L)

The Langmuir equation can be linearized as:

$$\frac{1}{q_e} = \left[\frac{1}{Q_m \cdot K_L} \right] \frac{1}{C_e} + \frac{1}{Q_m} \quad (12)$$

The essential characteristics of Langmuir isotherms can be expressed by dimensionless parameters known as separation factor, R_L , which is defined as:

$$R_L = \frac{1}{1 + K_L \cdot C_0} \quad (13)$$

Where; $C_0[mg/L]$ is the initial concentration of dye. The value of R_L thrown light on the nature of adsorption to be either unfavourable ($R_L > 1$), linear ($R_L = 1$), favourable ($0 < R_L < 1$) or irreversible ($R_L = 0$).

G.1.0.2 Freundlich Model

The Freundlich model [100] is the earliest known equation describing the adsorption process and can be written as:

$$q_e = K_F C_e^{1/n} \quad (14)$$

Where, K_F is a constant indicative of the relative adsorption capacity of the adsorbent and $1/n$ is a constant indicative of the intensity of the adsorption of dye onto the adsorbent or surface heterogeneity, becoming more heterogeneous as its value gets closer to zero. The Freundlich expression is an exponential equation and therefore, assumes that as the adsorbate concentration increases, the concentration of adsorbate on the adsorbent surface also increases. A value for $1/n$ below one indicates a normal Langmuir isotherms while $1/n$ above one is indicative of cooperative adsorption. The linear form of the Freundlich isotherm is shown as:

$$\log(q_e) = \log(K_F) + \frac{1}{n} \cdot \log(C_e) \quad (15)$$

To determine the maximum adsorption capacity, it is necessary to operate with constant initial concentration C_0 and variable weights of adsorbent, thus $\ln(Q_m)$ is the extrapolate value of

$\ln(q_e)$ for $C_e = C_0$. According to [101]:

$$Q_m = K_F \cdot C_0^{1/n} \quad (16)$$

Where, C_0 is the initial concentration of the solute in the bulk solution (mg/L) and Q_m is the Freundlich maximum adsorption capacity (mg/g). The Freundlich model assumes that the adsorbent surface is heterogeneous and is not restricted to monolayer adsorption. The possibility of multilayer adsorption and adsorption capacity of the adsorbent depends on the concentration of the adsorbent in solution at equilibrium.

G.1.0.3 Temkin Model

The Temkin isotherm model [102] assumed that the heat of adsorption of all the molecules in the layer decreases linearly with coverage due to adsorbent-adsorbent interaction, and that the adsorption is characterized by a uniform distribution of the binding energies, up to some maximum binding energy [103]. The Temkin isotherm has commonly been applied in the following form equation [104, 105, 105]:

$$q_e = \frac{R \cdot T}{b} \ln(K_T \cdot C_e) \quad (17)$$

The Temkin isotherm can be simplified to the following equation.

$$q_e = \beta \cdot \ln(K_T) + \beta \cdot \ln(C_e) \quad (18)$$

Where, $\beta = (R \cdot T)/b$ is the absolute temperature in Kelvin and R is the universal gas constant $8,314 J/mol \cdot K$. β is a constant related to the heat of adsorption [106, 107]. K_T is the empirical Temkin model proposes into account the effects of the interaction of the adsorbate and the adsorbing species. The model assumes that the heat of adsorption of all of the molecules in the layer would decrease linearly rather than logarithmically with coverage due to adsorbate-adsorbent interactions.

G.1.0.4 Dubinin-Radushkevich (D-R) model

The Dubinin-Radushkevich (D-R) model [108, 109] estimates the porosity apparent free energy and the characteristic of adsorption. The D-R isotherm does not assume a homogeneous

surface or constant sorption potential. The D-R model has commonly been applied in the following equation:

$$q_e = Q_m \cdot \exp(-K\varepsilon^2) \quad (19)$$

With linear form:

$$\ln(q_e) = \ln(Q_m) - K\varepsilon^2 \quad (20)$$

Where, K is a constant related to the adsorption energy Q_m the theoretical saturation capacity, ε is the Polanyi potential, calculated from equation:

$$\varepsilon = R \cdot T \cdot \ln\left(1 + \frac{1}{C_e}\right) \quad (21)$$

The slope of the plot of $\ln(q_e)$ vs ε^2 gives $K(\text{mol}^2/\text{K} \cdot \text{J}^2)$ and the intercept yields the adsorption capacity, $Q_m(\text{mg}/\text{g})$. The mean free energy of adsorption (E) defined as the free energy change when one mole of ion is transferred from infinity in solution to the surface of the solid, was calculated from the K value using the following relation equation [110]:

$$E = \frac{1}{\sqrt{2 \cdot K}} \quad (22)$$

G.2 Kinetic Study

Adsorption process are characterized by their kinetic and equilibrium behavior. The transport of the adsorbate at the solid-solution interface (adsorbent) and the attachment of the adsorbate surface determine the uptake rate of the adsorbate and thus the kinetics of the process [111].

The degree of purification that may be achieved, the approximate amount of adsorbent requirement to reach that degree of purification and the sensitivity of the process to the concentration of the solute are predicted by the isotherms. Many mathematical models have been studied in order to describe the kinetics of adsorption processes. The pseudo first order equation and pseudo second order equation are the widely used models for the adsorption kinetics of organic compounds [43].

A study of the kinetics of adsorption is desirable as it provides information about the mechanism of adsorption, which is important for the efficiency of the process. In addition, the design of an adsorption system for water treatment may be influenced or even controlled by the adsorption kinetics [112]. Several kinetic models for the liquid phase have been widely used to

describe experimental data. These include pseudo first order, pseudo second order and mass transfer/intra-particle diffusion model [113].

G.2.0.1 Pseudo First-Order Kinetic Model

The Lagergren first order model [114] is the earliest known and describing the adsorption rate based on the adsorption capacity. It is generally expressed as equation:

$$\frac{dq_t}{dt} = k_1(q_e - q_t) \quad (23)$$

Where, q_e and q_t are the adsorption capacity at equilibrium and at time t , respectively (mg/g), k_1 is the rate constant of pseudo first order adsorption (L/min).

This equation was integrated with the boundary conditions of $t = 0, q_t = 0$ and $t = t, q_t = q_t$, and rearranged to linear equation:

$$\log(q_e - q_t) = \log(q_e) - \frac{k_1}{2.303} \cdot t \quad (24)$$

The values of $\log(q_e - q_t)$ were linearly correlated with time (t). The plot of $\log(q_e - q_t)$ vs t should give a linear relationship from which k_1 and predicted q_e can be determined from the slope and intercept of the plot, respectively.

The variation in rate should be proportional to the first power of concentration for strict surface adsorption. However, the relationship between initial solute concentration and rate of adsorption will not be linear when pore diffusion limits adsorption process.

G.2.0.2 Pseudo Second Order Kinetic Model

The pseudo second order model given by Ho's equation [115]:

$$\frac{dq_t}{dt} = k_2(q_e - q_t)^2 \quad (25)$$

Where, $k_2(g/mg \cdot min)$ is the second order rate constant of adsorption. Integrating this equation for the boundary conditions of $t = 0, q_t = 0$ and $t = t, q_t = q_t$, is simplified as can be rearranged and linearized to obtain:

$$\left(\frac{t}{q_t}\right) = \frac{1}{k_2 \cdot q_e^2} + \frac{t}{q_e} \quad (26)$$

The second order rate constant were used to calculate the initial sorption rate, h , given by equation:

$$h = k_2 q_e^2 \quad (27)$$

If the second order kinetics is applicable, then the plot of t/q_t vs t/q_e should show a linear relationship. Values of k_2 and equilibrium adsorption capacity q_e can be calculated from the intercept and slope of the plots of t/q_e vs t . This model is usually attributed to the process that involves a mechanism of chemisorption. Estimate the load in equilibrium.

G.2.0.3 Elovich Kinetic Model

Elovich kinetic model equation is another rate equation based on the adsorption capacity, which is generally expressed as the following equation [116, 117, 118]:

$$\frac{dq_t}{dt} = \alpha \cdot \exp(-\beta \cdot q_t) \quad (28)$$

Where, α is the initial adsorption rate ($mg/g \cdot min$) and β is the adsorption constant (g/mg) during any one experiment. It is simplified by assuming $\alpha \cdot \beta \cdot t \gg 1$ and by applying the boundary conditions $q_t = 0$ at $t = 0$ equation becomes form as a linear equation:

$$q_t = \frac{1}{\beta} \cdot \ln(\alpha \cdot \beta) + \frac{1}{\beta} \cdot \ln(t) \quad (29)$$

Plot of q_t vs $\ln(t)$ should yield a linear relationship with a slope of $1/\beta$ and an interpretation of $1/\beta \cdot \ln(\alpha \cdot \beta)$. Thus, the constant can be obtained from the slope and the intercept of the straight line. The Elovich equation used for general application to chemisorption. The equation has been applied successfully to some chemisorption processes and has been found to cover a wide range of slow adsorption rates. The same equation is often valid for systems in which the adsorbing surface is heterogeneous.

G.2.0.4 The Intraparticle Diffusion Model (Weber-Morris)

The intraparticle diffusion [119, 120] model was used to identify the diffusion mechanism. According to this theory the adsorbate uptake q_t varies almost proportionally with the square root of the contact time $t^{1/2}$ rather than t .

The probability of intra particle diffusion is explored by using the following equation:

$$q_t = k_{dif} \cdot t^{1/2} + C \quad (30)$$

Where C is the intercept and k_{dif} is the intra particle diffusion rate constant. The values of q_t correlated linearly with the values of $t^{1/2}$ and the rate constant k_{dif} directly evaluated from the slope of the regression line. The values of intercept C provide information about the thickness of the boundary layer, the resistance to the external mass transfer increase as the intercept increase.

H Appendix 8.

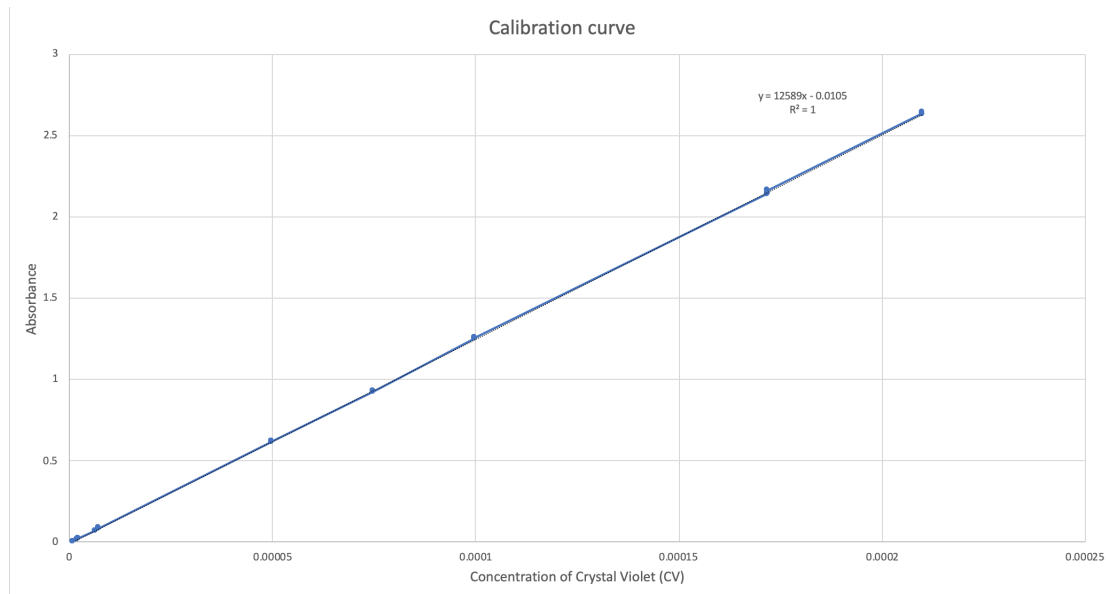


Figure 24: Relation between amounts of CV adsorbed at equilibrium (q_e) using different concentrations of SXQ-102 and SEM-205